Large Quasar Groups at Redshift ~ 2

By

Mark Peter Younger

A thesis submitted in partial fulfi ment for the requirements for the degree of Master of Philosophy at the University of Central Lancashire

August 2015

Declaration

I declare that while registered as a candidate for the research degree, I have not been a registered candidate or enrolled student for another award of the University or other academic or professional institution

I declare that no material contained in the thesis has been used in any other submission for an academic award and is solely my own work

Mark Peter Younger
December 2014

Abstract

This project aims to use the large public databases that are now becoming available in the Virtual Observatory. For my purpose two of the most important datasets for investigating Large Quasar Groups (LQGs) are the Sloan Digital Sky Survey (SDSS) and the 2dF Quasar Redshift Survey (2QZ). These have been used: to investigate stripe 82 of the SDSS; to discover large scale structures, specifically LQGs in the early universe; to investigate the expectation of finding LQGs at high redshift, and to investigate their properties in detail; to assess the compatibility of these structures with the concordance model in cosmology; to identify low redshift LQGs for investigation of the galaxy and cluster environments of quasars; to investigate whether correlations exist between LQGs and other cosmological sources, such as gamma ray bursters, the highest redshift quasars and radio galaxies catalogues; to probe the high-z LQGs with MgII absorbers from the Gemini data.

Using an algorithm for single-linkage hierarchical clustering, four LQGs have been found in the redshift range of 1.8 - 2.5. These four groups were tested for statistical significance using a convex hull approach, to calculate the overdensity. Each group was submitted to 1000 random simulations, no comparable structure was found from the random simulations. The algorithm was then applied to a greater redshift range of 0.6 - 2.5. The total number of groups found was 36, each group was tested for statistical significance using random simulations, each group found was to be real. To improve the statistical findings of these four high redshift groups, MgII absorbers from the Zue & Maynard catalogue of absorbers was used to investigate any MgII absorbers that were in the area of the four high redshift groups. The results found that many of the MgII absorbers lie in the peripherals of the groups, however, a few MgII absorbers lie within the groups themselves.

Acknowledgements

I wish to firstly thank my supervisor Roger Clowes, for his support throughout this project. I wish also to thank Catherine Harris for her support and understanding, and for keeping me sane throughout this endeavour, as well as our chats on how things should be. I would also like to thank the entire staff and students in the astrophysics department. And finally, I would like to thank my family for all their support given over the many years and their encouragement, while giving me the strength to continue and believing in me....

Contents

Acknowledgements iii

Contents iv

List of Figures vi

List of Tables vii

1 Background 1
- 1.1 Cosmology . . . 1
- 1.2 The Lambda model . . . 1
- 1.3 Quasars . . . 3
- 1.4 Evolution of quasars . . . 6
- 1.5 Large Quasar groups . . . 8
- 1.6 Expectation of finding large quasar groups . . . 9

2 Surveys 11
- 2.1 Surveys . . . 11
- 2.2 Soan Digital Sky Survey . . . 12
- 2.3 2dF Quasar Redshift Survey (2QZ)and the 2dF Galaxy Redshift Survey (2dFGRS). . . . 12
- 2.4 Chandra XMM-Newton . . . 13
- 2.5 Other surveys . . . 13

3 Identification of structure 15
- 3.1 Finding Structure . . . 15
- 3.2 Percolation . . . 15
- 3.3 Minimal Spanning Tree . . . 16
- 3.4 Friend of a friend . . . 17

4 The search for Large Scale Structure 18
- 4.1 The Group Detection Algorithm . . . 18

5 Results 25
- 5.1 High redshift LQGs 1.8 to 2.5 . . . 25
- 5.2 Summary . . . 27

6 MgII Absorbers 33

6.1 Gemini 34
6.2 Zhu & Maynard Catalogue 34
6.3 Results 35

7 Future Work **39**
7.1 Aims 39

A Tables of Results of the full list of quasars found **41**

B Tables of Results of the full list of Mg II Absorbers found **53**

Bibliography **59**

List of Figures

1.1 Cosmic Background from the Planck 2013 collaboration and WMAP data. The temperature fluctuations are so small, thus supporting the idea that the Universe is homogeneous on large scales. 2
1.2 The large scale structures seen by the 2df galaxy Redshift Survey. Showing the Universe on scales of $\sim$ 100 h^{-1}Mpc is isotropic. 3

4.1 Showing the non-uniformity of the whole of the SDSS survey with regards to the magnitude 24
4.2 Plot showing the uniform coverage of stripe 82, with regards to the magnitude 24

5.1 Plot of LQG 1, with 9 members and a redshift interval of 1.985 to 2.065 . 27
5.2 Plot of LQG 2 with 12 members and a redshift interval of 2.083 to 2.188 . 28
5.3 Plot of LQG 3 with 11 members and a redshift interval of 1.871 to 2.0 . . 29
5.4 Plot of LQG 4 with 8 members with a redshift interval of 1.871 to 1.927 . 30
5.5 A histogram showing the redshifts of all quasars in the SDSS DR7, which suggests that the peak occurrence can be seen to lie within the redshift interval 1.5 to 2.0 30
5.6 A histogram showing the frequency of the LQGs, with respect to the redshift of the groups. 32

6.1 Plot of LQG 1 and the Mg II Absorbers found within the redshift range of the LQG, the absorbers are in red 36
6.2 Plot of LQG 2 and the Mg II Absorbers found within the redshift range of the LQG, the absorbers are in red 37
6.3 Plot of LQG 3 and the Mg II Absorbers found within the redshift range of the LQG, the absorbers are in red 38

List of Tables

1.1 Values of cosmological parameters from ther Planck Collaboration 2013 data. . . . 3

4.1 Table showing the redshift bins and their calculated linkage scale for stripe 82. . . . 21

5.1 Table showing the four groups found at the redshift interval of 1.8 to 2.5, showing the centre of the groups the mean z, mean nearest neighbour separation (h^{-1} Mpc), density and the overdensity 26
5.2 Table showing the groups found at the redshift interval of 0.6 to 1.8, showing the centre of the groups the mean z, mean nearest neighbour separation (h^{-1} Mpc), density and the overdensity 31

A.1 Table showing the position, redshift and magnitude of each quasar in the LQGs 42
A.2 Table showing the position, redshift and magnitude of each quasar in the LQGs 43
A.3 Table showing the position, redshift and magnitude of each quasar in the LQGs 44
A.4 Table showing the position, redshift and magnitude of each quasar in the LQGs 45
A.5 Table showing the position, redshift and magnitude of each quasar in the LQGs 46
A.6 Table showing the position, redshift and magnitude of each quasar in the LQGs 47
A.7 Table showing the position, redshift and magnitude of each quasar in the LQGs 48
A.8 Table showing the position, redshift and magnitude of each quasar in the LQGs 49
A.9 Table showing the position, redshift and magnitude of each quasar in the LQGs 50
A.10 Table showing the position, redshift and magnitude of each quasar in the LQGs 51
A.11 Table showing the position, redshift and magnitude of each quasar in the LQGs 52

B.1 Table showing the position, redshift of the quasar, redshift of the absorbers and and the number of absorbers associated with the quasar. . . . 53
B.2 Table showing the position, redshift of the quasar, redshift of the absorbers and and the number of absorbers associated with the quasar. . . . 54

B.3 Table showing the position, redshift of the quasar, redshift of the absorbers and and the number of absorbers associated with the quasar. . . . 55
B.4 Table showing the position, redshift of the quasar, redshift of the absorbers and and the number of absorbers associated with the quasar. . . . 56
B.5 Table showing the position, redshift of the quasar, redshift of the absorbers and and the number of absorbers associated with the quasar. . . . 57
B.6 Table showing the position, redshift of the quasar, redshift of the absorbers and and the number of absorbers associated with the quasar. . . . 58

Chapter 1

Background

1.1 Cosmology

The standard cosmological model is based on the cosmological principle which assumes that our Universe is homogeneous and isotropic.

The Friedmann-Robertson-Walker metric is established through the cosmological assumption that our Universe is isotropic and homogeneous on the large scale. This therefore describes a homogeneous, isotropic expanding Universe.

$$ds^2 = (cdt)^2 - R(t)^2 \frac{dr^2}{1 - kr^2} + r^2 d\psi^2, \tag{1.1}$$

where r,ϕ are comoving coordinates, ds is the space time interval, t is the proper time, R(t) is the cosmic scale factor which describes the expansion of the universe, and k is a constant that takes the values -1, 0 ,1 accroding to space being, open , flat or closed. Observation of the Cosmic Microwave Background (CMB) confirms homogeneity to the level of ΔT/T $\sim$ O$(10)^{-5}$. This can be seen in fig 1.1. Observations of the large-scale structures (LSS) also confirm isotropy when smoothing the density field on scales of 100h^{-1}Mpc (Figure 1.2)

1.2 The Lambda model

The most widely accepted model of the Universe is the Lambda-Cold-Dark Matter model, and our current understanding of the Universe is encoded in this model. This model is capable of explaining the cosmic web and the Cosmic Microwave Background. The term Lambda refers to dark energy (Λ) which at present is believed to be the driving

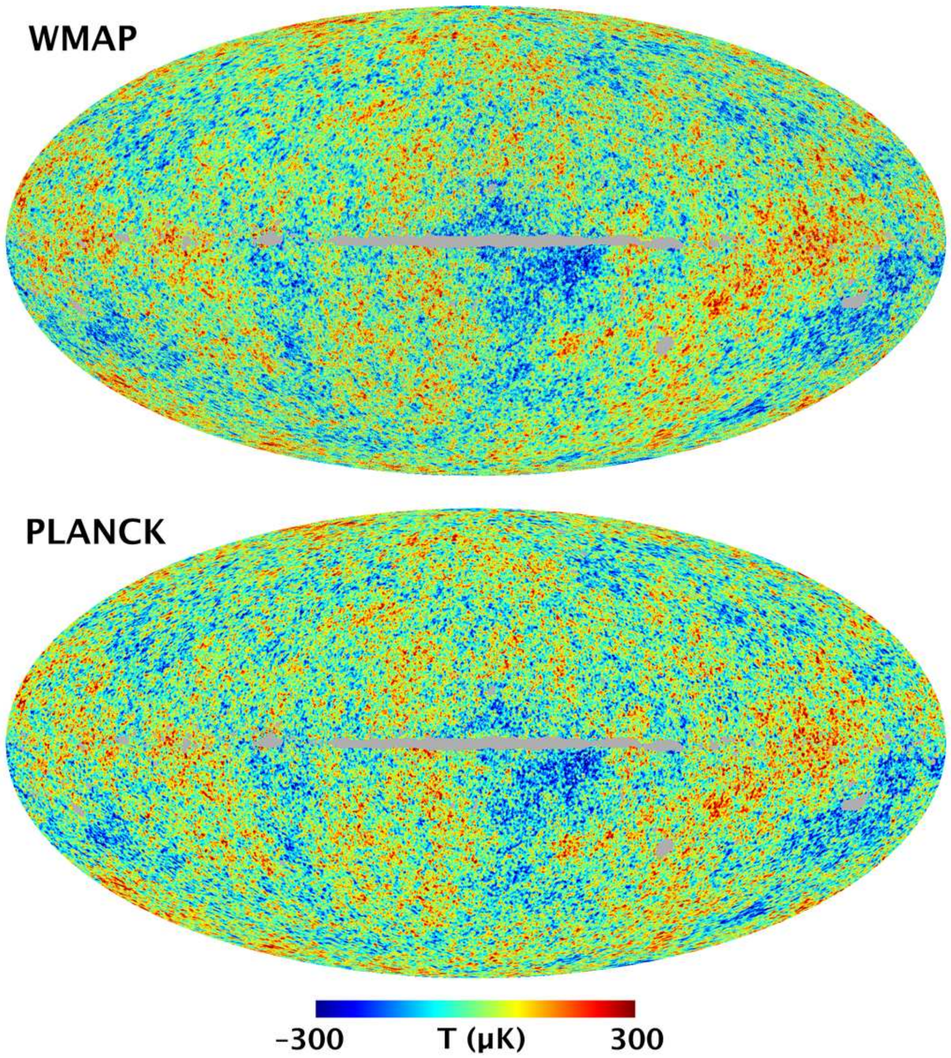

FIGURE 1.1: Cosmic Background from the Planck 2013 collaboration and WMAP data. The temperature fluctuations are so small, thus supporting the idea that the Universe is homogeneous on large scales.

force behind the expansion of the Universe at the present epoch. The cold dark mater in the model refers to where the dark matter is cold, where its velocity was non relativistic at the epoch where it decoupled from other constituents of the Universe. The ΛCDM model has several important parameters are Ω_{Lambda} (the dark energy density), Ω_M (the total matter density), Ω_b (the baryon density),H_O (the hubble constant), and σ_8 (the amplitude of density fluctuations an a scale of $8h^{-1}$, where $h = H_O/100kms^{-1}Mpc^{-1}$). In order to understand the evolution and structure of the Universe, the cosmological parameters of the ΛCDM model need to be determined to a high degree of accuaracy. There have a been a number of observations that have contributed to constraining the parameter values,e.g. Knop et al. (2003) in which they measusured distances from Type 1a supernova, the mapping of the CMB by WMAP (Spergel et al 2003), and more recently the Planck 2013 collaboration have investigated the cosmological parameters.

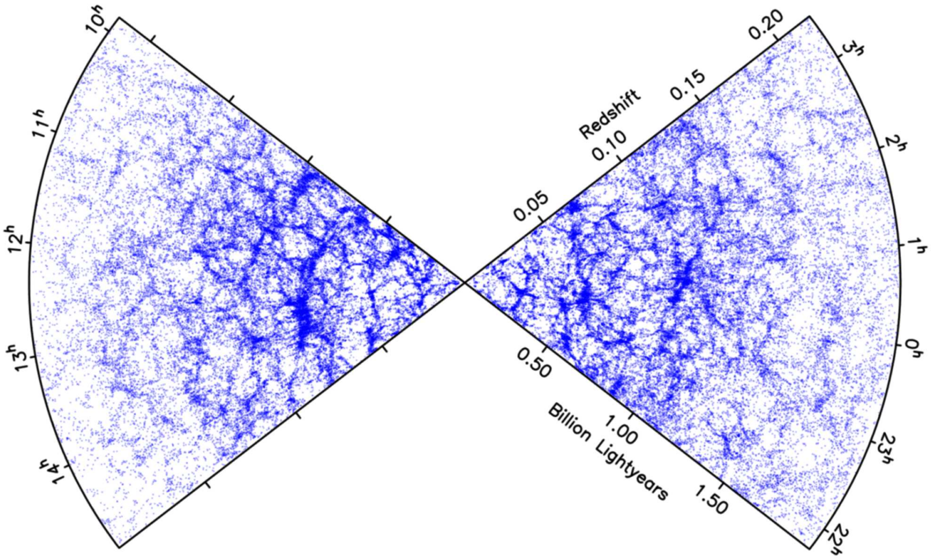

FIGURE 1.2: The large scale structures seen by the 2df galaxy Redshift Survey. Showing the Universe on scales of $\sim$ 100 h^{-1}Mpc is isotropic.

Parameter	Value	Description
H_0	$67.74 \pm .46$kms^{-1}Mpc	Hubble Parameter
Ω_m	$0.3089 \pm\ 0.0062$	Matter Density
Ω_b	$0.0223 \pm\ 0.00014$	Baryon Density
Ω_Λ	$0.6911 \pm\ 0.0062$	Dark Energy Density

TABLE 1.1: Values of cosmological parameters from ther Planck Collaboration 2013 data.

1.3 Quasars

High-redshift quasars are among the most luminous objects known and provide direct probes of the distant Universe when the first generation of galaxies and quasars formed. In recent years, over twenty z $\sim$ 6 quasars with have been discovered (e.g. Fan et al. 2000, 2001, 2003, 2004, 2006; Goto 2006). These luminous quasars are essential for understanding the accretion history of black holes (BHs), galaxy formation, and chemical evolution at very early epochs.

Quasars are relatively rare astronomical objects and hence, if they are distributed following galaxies, the presence of two or more such objects in a relatively small volume should be a good indicator of a rich environment. Actually, in structure formation scenarios with bias between baryonic and dark matter distributions (e.g., Kaiser 1984) it is expected that high redshift objects form in large high redshift density fluctuations and, therefore, such correlation between quasar concentration and clusters is somewhat expected, unless for some reason, quasars avoid clusters. However, most observational evidence shows that high redshift quasars do tend to follow the overall large-scale structures. Whether quasars inhabit or not high density regions at low redshifts is a subject of dispute. Coldwell et al. (2002), for example, claim that at $0.1 \leq z \leq 0.25$, quasars (both radio loud and radio quiet) tend to reside in low density regions. On the other hand Mullis et al. (2004), using a sample of X-ray selected quasars, conclude that those objects trace closely the underlying mass distribution.

Sochting et al. (2002) also points out that $0.2 \leq z \leq 0.3$ quasars follow the large-scale structure traced by galaxy clusters, but they also note the complete absence of radio–quiet QSO's at the very centre of galaxy clusters. At higher redshift, however, most observational results suggest that quasars prefer groups or clusters (Hall & Green 1998; Wold et al. 2000, 2001). One very convincing example is the structure found by Haines et al. (2001) at $z = 1.226$ around a radio-quiet quasar belonging to a large quasar structure (Clowes & Campusano 1991, 1994).

The same behaviour appears to be followed by radio-loud quasars. A good example is the work by Sanchez & Gonzalez-Serrano (2002), who found a highly significant excess of galaxies around radio-loud quasars at $1.0< z <1.6$. Tanaka et al. (2001) also points in the same direction by reporting an overdensity of galaxies around a quasar concentration at $z \sim 1.1$. An exception is the work by Coil et al. (2007) who, through an analysis of the clustering of quasars and galaxies at $0.7< z < 1.4$, concluded that quasars and blue galaxies are found in the same environment, which differs from that occupied by the red galaxy population.

Regarding specifically quasar pairs, Zhdanov & Surdej (2001) found statistically significant excess of high redshift quasar pairs with separations between 1 and 5 Mpc in projected distance. This suggests that such quasar pairs belong to sizable physical structures (precursors of today's clusters and superclusters of galaxies) and therefore, they can be used as tracers of high redshift large-scale structures. Going to even larger redshifts, Djorgovski et al. (2003) found that a quasar pair at $z = 4.96$ is associated with a large-scale structure. Thus, an interesting method to search for high-redshift clusters and other large-scale structures is examining the environment inhabited by quasar pairs and triplets.

Given the hypothesis that LQGs (Large Quasar Groups) denote the precursors of superclusters, the assumption is made that the quasars in LQGs will follow the LSS (Large Scale Structure) in galaxies. The success in establishing this hypothesis, would have particular advantages in investigating the development of structure in the Universe because the quasars can be more readily detected than galaxies. The high density quasars within LQGs can also lead to observational efficiency when investigating the large and small scale enviroments of quasars and consequently the mechanisms for quasar formation.

Cosmologically, quasars can now be explained as one spectacular stage of an evolutionary process, possibly initiated by gas-rich mergers, that ultimately helps redden elliptical galaxies (Hopkins et al. 2006, 2007a). Quasars rank among the most luminous objects in the universe and are believed to be powered by Super Massive Black holes (SMBHs). They constrain the formation and evolution of galaxies and SMBHs throughout time.

The similarity between star formation history and the evolution of quasar abundances suggests an intriguing link between galaxy formation and black hole growth. As quasars are highly luminous they are important cosmological probes for studying the first galaxies, star formation history, metal enrichment in the early universe, the growth of the first SMBHs, the feedback from quasars and black holes in galaxy evolution and the epoch of reionization. The accretion of matter onto a black hole is the most efficient method for converting matter into radiation ($\sim$10 percent c.f 0.7 percent for nuclear fusion) and appears to be the only method capable of producing the observed luminosity and spectra.

Quasars have a distinctive spectra which makes them relatively easy to find, with broad emission lines superimposed on a featureless continuum spectrum with a power law, over a large range of frequencies from X-ray to radio. This spectral index results in a colour much bluer in U - B than most common stars, with the expectation of white dwarfs.

Using a UVX selection of sources with U - B $<$ -0.3 gives a nearly complete list of z $\sim$ 2.2 quasar candidates which can then be classified through spectroscopic studies. However this method breaks down for high redshift quasars, as the strong Lyman alpha lines moves into the B-band, and reddens the U - B colour. The most generally accepted triggering mechanism for quasars is the galaxy merger picture, in which it is assumed that in the centre of a certain fraction of galaxies exists a supermassive blackhole, which for most of the time remains in a quiescent state accreting at a low rate.

When a galaxy containing such a black hole collides and merges with another galaxy it is possible that, if the second galaxy passes very close to the black hole then significant amounts of matter are captured by its gravitational field, and in which case the black hole will start to accrete matter at a much increased rate ($\sim 100 M_{\odot}\ yr^{-1}$ and become a quasar with an expected lifetime of the same order as the merger time scale $\sim 10^8$ years). Several results support this theory, the first being observational with excess numbers of companion galaxies for the quasar host galaxy found.

1.4 Evolution of quasars

Through observations and theoretical modelling, mergers between galaxies occur on a regular basis. Those involving gas rich progenitors would be increasing more common towards higher redshifts in hierarchical cosmologies and it has been suggested that this might explain the observed evolution of quasars.

The number density of merging events producing black holes of the size $10^9_\odot$ decreases at high redshift simply because such massive objects form very late. The number density producing smaller black holes does increase at high redshift, but the effect is to small to explain the observed increase in the quasar space densities from z = 0 to z = 2. Another hypothesis is that the black holes run out of fuel at late times. It has been found in models used by Kauffmann and Haehnelt (1999), that the amount of gas accreted by merged blackholes of a given mass increases by a factor ~3 from z = 0 to z = 1, but in their models the quasars do not run out of fuel because the gas is exhausted at the present, but with the cool gas being converted into stars more efficiently at low redshift. They assume that the rest mass energy of the accreted material is radiated in the B-band, which results in the following transformation between the accreted gas mass M_{acc} and the absolute B-band magnitude of the quasar at the peak of its light curve $M_B(peak) = -2.5log(\frac{\epsilon_B M_{acc}}{t_{acc}})$-27.45 and would produce inflows of gas through gravitational torques, which would cause star bursts, these star bursts would rapidly fuel black hole growth.

For most of the period over which blackhole growth occurs the quasar would be optically buried, but X-ray sources would explain the presence of non-thermal point sources. As the black hole mass and radiative output increase, a critical point is reached where feedback energy starts to expel the gas fueling the accretion, and therefore for a short time the galaxy would be seen as an optical quasar with a B-band luminosity. This phase of evolution is brief $\sim 10^7$yr, owing to the explosive nature of the final stages of the black hole growth, the gas responds to the feedback energy from the exponentially black hole. This feedback terminates further black hole growth, leaving behind a remnant that resembles an ordinary galaxy containing a dead quasar (Hopkins et al. 2005).

It has become clear that black holes play a key role in the evolution of galaxies, and that most galaxies have super massive black holes in their nuclei (Richstone et al. 1998, Ferrarese and Ford 2005), and that as these black holes power AGN (Active Galactic Nuclei), there are strong observed correlations between black hole mass and galaxy properties such as the stellar velocity dispersion in the bulge (Gebhardt et al. 2000, and Ferrarese and Merritt 2000), that indicate some form of feedback or connection between the growth of black holes and their parent galaxies. It still remains unclear how galaxies and AGN co-evolve and what impact the AGN have on the evolution of their host galaxies, as is still unknown what the accretion mechanism is for AGN and what their fueling source is.

Theoretical models of AGN formation and evolution can yield measurably different predictions for the local environments and clustering properties of AGN. Kauffmann and Haehnelt (2002) use a semi analytic model in which AGN are fueled by galaxy mergers, where the peak AGN luminosity depends on the mass of gas accreted by the black hole, which in turn depends on the halo mass. This leads to a prediction that the brighter AGN reside in more massive halos such that the AGN clustering amplitude should be strongly luminosity dependent. This model is not supported by observations, which in general show a lack of a strong correlation between the AGN clustering amplitude and the luminosity except at the very bright end (Croom et al. 2002, Shen et al. 2008)

Hopkins et al. (2005,2008) present an alternative model in which bright and faint AGN are similar in physical systems but are in different stages of their life cycle. This model predicts that faint and bright AGN should reside in similar mass dark matter halos and that quasar clustering should depend only weakly on luminosity (Lidz et al. 2006).

This general prediction agrees well qualitatively with observations of quasar clustering but the model also predicts that lower luminosity AGN should have an equal or lower clustering amplitude than bright AGN, but Coil et al.(2009) find that this is not well supported when comparing their results for non-quasar X-ray AGN with their results for quasars in Coil et al. (2007). In the model presented by Hopkins et al. (2008) the AGN are detected in X-rays while obscured by dust just after a major merger, before undergoing an optically-bright quasar phase a short time later. Coil et al. (2008) find that this picture is not well supported by their results. The semi-analytical model of Croton et al. (2006), combines a prescription of merger-driven black hole growth similar to Kauffmann and Haehnelt (2000) with an independent mode for hot gas accretion in large halos which accounts for the fueling of lower luminosity AGN in massive halos.

This models assumes that some fraction of cold gas must be present to trigger a bright quasar phase during a galaxy merger, the black hole itself must also be massive such that the luminosity remains sub-Eddington. Quasars in this model can be strongly clustered at high redshift when cold gas fractions are presumably high, but as their host dark matter halos grow cooling becomes more inefficient as the viral temperature of the halo increases and the cold gas supply is suppressed above a given threshold mass, quasars will only be found in halos below the threshold mass and thus gas free red galaxies are not expected to shine as quasars. Only those mergers that occur in lower mass halos presumably outside of group environments at $z < 1$ will contain sufficient cold gas to fuel a quasar, this model therefore predicts that quasars should cluster similarly to massive star forming galaxies at a given redshift where both star formation and quasar activity are fueled by cold gas, Thacker et al. (2008) present a model for quasar fueling and feedback that quantitatively matches observations of quasar and X-ray clustering reasonably well. In their model bright AGN are the result of mergers and are augmented by feedback from AGN outflows, they do not present predictions for z $<$ 1.2 but their model matches well the observed clustering of quasars at z = 1.5 - 2.

1.5 Large Quasar groups

Large Quasar Groups (LQGs) have memberships $\sim$ 5–25 and proper sizes at the present epoch $\sim$ 70–250h^{-1}Mpc, the first group discovered by Webster which consisted of 4 quasars at z $\sim$ 0.37 with an extent of $\sim$100h^{-1}Mpc (Webster 1982) One of the largest currently known groups is one found by (Crampton, Cowley & Hartwick in 1989), and consists of 23 quasars at z $\sim$ 1.1. Two groups of quasars selected by Automatic Quasar Detection (Clowes 1986) from objective prism plates (Clowes and Campusano 1991), were found using the Minimal Spanning Tree (MST) cluster finding algorithm, one consisting of 18 quasars (Clowes & Campusano 1991;1994; Graham,Clowes & Campusano 1995) at z $\sim$ 1.3 with an extent of $\sim$ 100 - 200h^{-1}Mpc and another one of 10 quasars (Graham,Clowes & Campusano 1995) with dimensions of $\sim$ 120 x 90 x 20h^{-1} Mpc at a higher redshift of z $\sim$ 1.9. Kromberg et al. (1996) found 12 groups with one group containing 23 members, but this was from several homogeneous surveys put together. Doing this would lead to differences in accuracies in coordinates and redshift, this would therefore produce a data set that is inhomogeneous (Kromberg, Kravtsov & Lukash 1996).

Pilipenko (2007) found 20 groups from the 2dF redshift survey. The fact that there have only been $\sim$ 40 groups found so far to date suggests that this is a rare phenomenon, although this is primarily due to the lack of large faint homogeneous surveys capable of detecting such groups, even with the advent of surveys such as the SDSS which consists of $\sim$ 70 000 quasars and the 2dF quasar survey (Croom et al. 1998) which consists of $\sim$ 30000 quasars. The SDSS survey contains many non-unformites and to produce a uniform data set requires the reduction of the amount of quasars (Richards et al. 2006). The 2dF covers two 75 $^{\circ}$ x 5° declination strips, but this narrow geometry may limit its ability to detect LQGs.

Clowes et al. (2012) present two groups from the SDSS DR7 quasar catalogue (Schneider et al. 2010), one of these groups is from a previously known group the Clowes & Campusano (1991) group with 34 members. The second group was a new group found, with a membership of 38 quasars. With these two groups they suggest that they are only marginally compatible with homogenity. However, in Clowes et al. (2013) they find a group with membership of 73 quasars, with an average redshift z$\sim$ 1.2, with this group they suggest that due to its size it has incompatibility with the Yadav et al. (2010) scale of homogeneity for the concordance cosmology and suggest that the group challenges the assumption of the cosmological principle. However Pilipenko (2014) dismisses these findings and suggests the group does not break the homogeneity scale. The known quasar groups appear to be of the same scale as large-scale structures such as the Great wall or Great attractor, and it has been suggested (Kromberg and Lukash 1996; Wray et al 2006) that quasar groups are progenitors of these large-scale structures. As individual quasars appear to reside in galaxy clusters it does not appear unreasonable that a group of quasars would trace a series of clusters, or a supercluster such as the aforementioned structures.

1.6 Expectation of finding large quasar groups

The detection of LQGs at $z \sim 2$ might be assisted by quasar activity being at its highest then. Conversely, the rather bright limiting magnitude, $i \leq 19.1$ of the main "low-redshift" quasar survey of the SDSS will not be an advantage. The best opportunities will be in those areas of the SDSS such as stripe 82, as used here, for which deeper coverage has also been acquired, principally to address the higher redshifts, $\sim$ 3–7.

Information is sparse on the theoretical expectations for detecting large-scale structures at $z \sim 2$. The simulations of Einasto et al. (2008) suggest that few clusters would be found at such redshifts. There have nevertheless been successful detections of galaxy groups and structures of Lyman-alpha emitters (LAEs) at $z \sim 4$, found by Shimasaku et al.(2004). But their results do suggest that the birth of LSS is very early in the history of the universe, in which they also suggest that LAEs are strongly biased against dark matter. Doroshkevich et al.(1999) used N-body simulations to investigate what they called rich structure elements (RSEs) that contain $\sim$ 40% of the mass at the present epoch. They find that at z $\sim$ 1 the fraction of the mass in RSEs is $\sim$ 20% and that at z $\sim$ 3 it is negligible, but give no fraction for z $\sim$ 2.

In recent years numerical simulations are being more used to investigate the formation and evolution of LSS, as the SDSS and 2dF have characterized the spatial clustering and physical properties of low red shift galaxies more accurately than other surveys, and as with all surveys the primary goal is to understand galaxy formation and to see if these models fit in with the concordance model of formation. Unfortunately the SDSS does not go deep enough and concentrates really only on the low redshift end, the 2dF catalog contains 25 000 quasars in two 75° x 5° areas. To get accurate predictions of clustering requires simulations of extreme dynamic range, encompassing large volumes of objects at high redshifts.

Two such simulations may be the answer, the Millennium simulation which was carried out by the Virgo Consortium, which uses N=21604^3 particles from redshift z = 127 to the present in a cubic region of $500h^{-1}$ Mpc (Springel V et al. 2005). So far the Millennium simulation has been used to recreate the evolutionary histories for approx 20 million galaxies as well as examining the super massive black holes which may drive quasar activity (Lemson G Virgo Consortium 2006). It also enabled the implememtation of physical models for the formation and evolution of galaxy/AGN populations throughout a large and representative cosmological volume (Croton et al. 2006; Bower et al. 2006). The millenium II simulation have focused on larger volumes, $L_{box} \gtrsim 1000\ h^{-1}$ Mpc, this will allow for the production of mock catalogs for the next generation of galaxy surveys (Fosalba et al. 2008 ;Teyssier et al. 2009).

The Horizon simulation is the largest N body simulation ever performed, they will simulate 13.7 Gyr long evolution of N = 4096^3 dark matter particles in a $2h^{-1}$ Gpc periodic box, in which the goal of this simulations is to generate a full mock sky catalog with realistic galaxy distribution up to z $\sim$ 1 and a deeper catalog of 500 sq degrees up to z $\sim$ 7 in which they will be approaching the cosmological horizon. With both these projects it will become much easier to simulate large-scale structure at high redshifts.

Recently Wray et al. (2006), used simulations to investigate super-clusters from z =0 to z= 2, they find that the abundance of super clusters decreases rapidly with increasing redshift. They suggest that there are many more superclusters at low z due to there being more clusters formed at the present that gravitated to form super-clusters. Komberg et al. (1996) suggested that a high abundance of LQGs between z $\sim$ 1 and z $\sim$ 2 may indicate pre-superclusters, this seems to be in agreement with the results found by Wray et al. (2006).

Different cosmological models and different choices of cosmological parameters produce different forms of large-scale structure and different evolutionary paths. So the presence of large quasar groups in the early Universe can put constraints on acceptable choices of cosmological model, however there is a major obstacle in the use of quasars, the question of the bias between the quasar and the mass distributions. If quasars have a high bias, then they only form in the deepest gravitational potential wells, they then appear to be more strongly clustered than the underlying mass distribution. If the quasar mass bias depends on other environmental factors then the relationship between quasar clustering and mass clustering will be complicated further.

Chapter 2

Surveys

2.1 Surveys

The main goal is to use the quasars to probe the large-scale structure of the Universe over a range of scales 1 to 1000 h^{-1}Mpc . Clustering of quasars on small to intermediate scales supplies a wealth of information on large scale structure, as quasars still only give us a way of directly determining the three dimensional clustering of high redshift objects, within a large enough volume for it to be truly representative. The shape and amplitude of the two point auto correction function are determined by two factors. Firstly, the distribution of matter in the Universe, which depends on the physics, such as the growth of structure via gravitational instability and the initial spectrum of fluctuations. The second factor is the complex and generally non linear physics which occurs during galaxy and quasar formation. But the photometric colour selection used to construct the survey becomes inefficient at $z > 2.5$ (Croom et al 2004) as there is concerns about selection efficiency possibly mimicking cosmological structure. The principle goal of all these surveys is to shed light on how galaxies form, to test the current paradigm for the growth of structure, as well as searching for the signatures which may give rise to the nature of dark matter and dark energy. These goals can be achieved if the theoretical predictions can be compared to the accurate measurements made by these surveys. Unfortunately there are two problems that have eluded such predictions, the accurate estimates of clustering require simulations of extreme dynamic range, encompassing volumes large enough to contain populations of rare objects such as rich cluster galaxies and quasars, yet resolving the formation of the individual low luminosity galaxies, the other problem is that, critical aspects of galaxy formation physics are uncertain and beyond the reach of direct simulation.

2.2 Soan Digital Sky Survey

SDSS has produced both imaging and spectroscopic surveys over a large area of the sky, a dedicated 2.5m telescope equipped with a large format mosaic ccd to image the sky in five optical bands and two digital spectrograph's to obtain the spectra of galaxies and quasars , York et al. (2000). The five optical bands u', g',f', i', z', with effective wavelengths of 3590Å, 4810Å, 6230Å, 7640Å, 9060Å,(Fukugita et al. 1996). The primary goals of the SDSS survey are to investigate the evolution of the quasar luminosity function,and the spatial clustering of quasars as a function of redshift. To achieve this it is necessary for there to be a large sample of quasars covering a broad range of redshifts and chosen with a well defined uniform selection criteria. This survey will increase the number of known quasars by a factor of 100 over other surveys such as the large bright quasar survey Hewett et al. (1995). The SDSS survey has a high completeness fraction from z = 0 to z $\sim$ 5.8. Searches from the very high redshifts quasars require spectroscopy outside of the normal SDSS operations (Fan et al 2001). At low redshift the design of gap separation of the u' and g' filters allows for the difference between objects with power law spectral energy distributions as with quasars at $z < 2.2$ and objects that are strongly effected by the balmer decrement. The quasar selection code is as follows , objects with spurious problematic flux's in the imaging data are rejected, point source matches to FIRST radio sources are preferentially targeted without reference to their colours, these sources that have remained after the first step are then compared to the distribution of normal stars and galaxies in two distinct 3D colour spaces. However, the SDSS contains many inhomogeneities, which would in turn give uncertain results, but, stripe 82 has been repeatedly surveyed thus allowing for a much more uniform area. For further information on the operation of the SDSS see Richards et al. (2002)

2.3 2dF Quasar Redshift Survey (2QZ)and the 2dF Galaxy Redshift Survey (2dFGRS).

The 2dF QSO redshift survey 2QZ has compiled a homogeneous catalogue of $\sim$ 25000 QSO's using the Anglo-Australian telescope AAT 2-degree field facility (Taylor,Cannon and Watson 1997), catalogue will constitute a factor of $>$ 50 increase in numbers to a equivalent flux limit over previous data sets. The main goal is to use the quasars to probe the large scale structure of the Universe over a range of scales 1 to 1000 h^{-1}Mpc out to high redshift $z < 3$. However, the area used by the 2dF quasar redshift survey, is a small area and thus may not produce the required catalogue for a search of LQGs.

2.4 Chandra XMM-Newton

The XMM-Newton survey, has the greatest collecting power to date, with a total collecting area of 120 square meters spread across three individual X-ray detectors. Since it's launch in 1999, it has been observing the interaction of blackholes with their surroundings, supernovae, origin of powerful gamma-ray bursts, and the evolution of the Universe by looking back at it's origin and examining the X-ray properties of quasars. With it's high throughput and ability to make long time series observations, it is returning outstanding data on simultaneous X-ray, UV, and optical emission. The X-ray studies of the high energy phenomena and processes in galactic bulge provide vital insight into our understanding of galaxy formation and evolution. The XMM-Large scale structure survey (XMM-LSS) is an X-ray survey aimed at studying the large-scale structure of the Universe by the use of the XMM-Newton satellite, this survey will map out the locations of extragalactic sources relative to large scale structure as traced by the X-ray emission. This is of particular interest as radio galaxies and radio loud AGN show strong and complex interactions with their small and larger scale environment, different classes of radio galaxies are suggested to lie at different places with respect to the large scale structure (Tasse et al 2006). Chandra was launched in 1999, and is designed to observe X-rays from high energy regions of the Universe, such as the remnants of exploded stars. It has also found that the luminosity dependent density evolution, where lower luminosity systems peak at lower redshifts, is in fair agreement with the observations. The luminosity dependent evolution is consistent with scenarios suggesting that lower luminosity systems are associated with star formation activity and peak at $z \sim 1$, while the more powerful quasars evolve out to higher z (Georgakakis et al. 2006). The unified model for active galactic nuclei (Antonucci 1993), has predicted that a large population of heavily obscured powerful quasars, called type 2 quasars, which might dominate black hole growth (Martinez-sansigre et al 2005) have been missed by optical surveys. The hard X-ray emission is less biased by obscuration, making the hard X-ray surveys a good approach to searching for type 2 quasars. Recent deep wide-area X-ray surveys performed by Chandra and XMM-Newton have revealed a number of such sources(Fiore et al. 2003; Caccianiga et al 2004). Using the Chandra Deep Field surveys it has been confirmed that there is a large population of obscured quasars, Wang et al. 2007 found that in the CDF-South $\sim 75\%$ of the XMM-Newton sources are obscured.

2.5 Other surveys

LSST also known as the Large Synoptic Survey Telescope, is a ground based 8.4-meter, 10 square-degree-field telescope, that will provide digital imaging of faint astronomical objects across the entire sky. These images will be able to trace apparent distortions in the shapes of remote galaxies produced by lumps of dark matter, providing multiple tests of the mysterious dark energy. VISTA (Visible and Infrared Survey Telescope for Astronomy) is a 4-meter class wide field survey telescope for the southern hemisphere, equipped with a near infrared camera containing 67 million 0.34 arcsec pixels and available broad band filters at Z,Y,J,H,Ks, and a narrow band filter at 1.18 micron. The site, telescope aperture, wide field, and high quantum efficiency detectors will make VISTA the worlds outstanding ground based near-IR survey instrument.

Chapter 3

Identification of structure

3.1 Finding Structure

Finding large scale structure, the distribution of mass in the Universe can be represented as a time dependent continuous scalar field of the mass density contrast δ defined by

$$\delta(x,t) = \frac{\rho(x,t) - \bar{\rho}}{\bar{\rho}(t)}$$

,

where $\rho(x,t)$ is the density at position x and time t and $\bar{\rho}(t)$ is the mean density at the same epoch. The mathematical tools used for analyzing delta can be divided into three categories. The first category deals with the identification of structures, the second category measures the strength of the clustering, and the third category deals with the topology of the distribution. To see the detailed mathematical treatments see Peacock (1999), Peebles (1993).There are several methods for identifying structure from large catalogs, three of them are minimal spanning tree, friend of a friend and percolation.

3.2 Percolation

Percolation analysis, uses a set of points in scattered in a cubic volume of space of side L containing $N >> 1$ objects. Place a sphere of size r = bl/2, where l = $L/N^{(1/3)}$, which is the mean inter-point distance and b is a dimensionless percolation parameter. When the spheres around each point overlap they then become friends, and chains of overlapping spheres connect friends of friends. If b is large all points are joined and if b is small, all points are isolated. As b increases the number of separate groups decrease from N to 1. There is a critical value, b_c when this is achieved then one group forms that bridges the sample cube thus achieving percolation. The value of this b_c depends on N, L and on the geometry of the spatial points. For large N the Possion distribution' of points show that the mean $b_c \sim 0.87$ (Coles and Lucchin 1995). In a regular lattice with planes parallel to the sample cube, with a uniform distribution of points it can be clearly shown that $b_c = 1$. In a sheet like distribution of the same number of points at separation delta arranged in parallel planes of thickness $h << L$, each plane will percolate when $b_c = (\mathrm{h/delta})^{1/3} < 1$. For a distribution in straight strings of diameter $h << L$ percolation along each road will occur when $b_c = (h/delta)^{2/3} << 1$. For the clustering of points in small cubes of side $h << L$ separated by distance delta it can be shown that $b_c = 1$. The groups formed by friend of friend at different values of b both identifies and characterizes structures in the point set.

3.3 Minimal Spanning Tree

The minimal spanning tree (MST) is a geometric construct originating in graph theory and was introduced by (Kruskal 1956 and Prim 1957) and was first introduced into astronomy by Barrow et al. (1985) to describe the intrinsic patterns in the galaxy distribution and has been used greatly in the studies of clustering (Adami and Mazure 1999; Broadbeck et al 1998; Coles et al 1998; Graham, Clowes and Campusano 1995). The MST is a tool from graph theory which can be used to quantitatively identify clusters of objects in a manner analogous to that which is performed by the eye. The information contained in a percolation analysis is also contained in a MST analysis, the MST analysis can provide more information more efficiently than friend of friend (Bhavsar and Splinter 1996). A spanning tree is defined as a graph of edges connecting all objects in a set with no closed paths. The edge lengths may be specified in the natural dimensions of the data or they may be in some other data that represent the strength of connection between objects (Krzewina and Saslaw 1996). In the spanning tree the sum of the edge lengths is minimized. The tree can be pruned of short branches to highlight structural backbones, it can also be divided into sub trees by removing edges longer than some length for example to maximize the number of sub-trees that appear. One of the powerful features of MST is that it can identify structures whose characteristic size is similar to the survey size.

3.4 Friend of a friend

Kromberg et al. (1996), friend of a friend is a cluster analysis method, the kernel of this method is an objective, automated procedure to separate a set of objects into individual systems. Draw a sphere of radius R_{cl} (clustering radius) around each sample point i.e. quasar, if there are other quasars within the sphere, they are considered to belong to the same system, these quasars are called friends, then draw spheres around these new neighbours, continue to this using the rule any friend of my friend is my friend, this stops when there are no more neighbours or friends to add to the system. In these systems every object has at least one neighbour at a distance of 1 less R_{cl}. In this method the choice of cluster radius is crucial if R_{cl} is to small then it will only detect close pairs or triplets, if R_{cl} is to large then all the quasars join to form a huge system.

Chapter 4

The search for Large Scale Structure

4.1 The Group Detection Algorithm

The procedure to find LQGs has been applied to stripe 82 of the SDSS. Stripe 82 has been repeatedly imaged by SDSS, from 1998 to 2005, to permit deeper studies and measure variability. Schawinski et al.(2010), have used stripe 82 to examine the role of mergers in early type galaxy evolution, in the past surveys did not reach sufficiently deep surface brightness; due to the deeper imaging from stripe 82, results have become more reliable.

No real attempt have been used to incorporate the whole of the DR7 due to potential difficulties arising from the non-uniformities, in which these non-uniformities of a factor of ~ 2 appear in the surface density at all redshifts on scales $\sim$ a few degrees. The non-uniformities arise from the superposition of the low redshift strand and areas with different selection limits, algorithms and completeness. These potential difficulties arising from the non-uniformities may be illustrated by Pilipenko (2007), who finds fainter LQGs from the 2QZ data (Miller et al. 2004) but finds no groups beyond doublets and triplets in the SDSS, but this may also be because of his choice in linkage length, which is less than I have used.

The identification of LSS by algorithms can be quite subtle, especially concerning the effective and objective specification of factors such as the linkage scale and overdensity. The mean nearest neighbour separation for a Poisson distribution can be used to set, approximately, the lower limit and the expected radius for a Poisson distribution (Marti′nez & Saar 2002) and can be used to set, approximately, the upper limit.

With this investigation the use of a single linkage hierarchical clustering has been used, which is effectively the same as the use of the minimal spanning tree (MST). The algorithm used to locate these groups was accomplished by using a statistical and programming package called R. (This is a GNU project, available free on-line and is designed for statistical programming and graphics). The algorithm selects quasars from the area selected with a redshift interval of no greater than 0.4, each redshift bin overlapped the next bin by 0.1, at a linking length found from the nearest neighbour. The use of a graphical program GGobi, is used to visually investigate the groups in 3D, to examine any sub-clustering of the groups and the morphology of the groups.

I have used the SDSS DR7 quasar database (Schneider et al. 2010) to test for LQGs but upon investigating the entire SDSS database it was found that it contains many inhomogeneities, Richardson (2006). To find real structures and determine their statistical significance, any inhomogeneities must at least be understood, as these inhomogeneities will make the results uncertain. Surveys collect inhomogeneities at many construction stages, including imaging from variations in sky brightness, the definition of point or extended sources in the reddening and the density of stellar contaminants; Spectroscopy from variation in S/N across each tile. To reduce the inhomogeneity it was therefore necessary to produce a uniform coverage of the entire database. By constraining the magnitude psi to the range of ≤ 19.1, this produced a more uniform survey, but reduced the amount of quasars available for the search and the amount of groups found. Figure 4.1 shows the non-uniformities of the whole of the SDSS survey. In comparison Figure 4.2 shows just stripe 82 and the uniform coverage that stripe 82 produces.

The detection algorithm consists of the following steps.

(1) The selection of all quasars within the selection parameters RA, Dec, z, magnitude and nearest neighbour distance in which the choice of the linkage scale is important. If r_{link} is too small then only units with a few members, such as doublets and triplets, will be detected. If r_{link} is too large then many or most of the quasars will be clustered together. The adopted linkage scale has been set by the nearest neighbour separation expected for a random distribution.

The probability of no neighbour in the range 0 to r, is found from the Poisson distribution,

$$P(x) = \frac{e^{-m}m^x}{x!} \tag{4.1}$$

For x=0

$$P(0) = e^{-m} \tag{4.2}$$

where m is the expectation value corresponding to r.

$$P(0) = e^{-\frac{4N\pi}{3}r^3} \tag{4.3}$$

Where N is the volume density

$$dP' = 4N\pi r^2 dr. \tag{4.4}$$

Hence

$$dP = 4N\pi r^2 e^{-\frac{4N\pi}{3}r^3} dr \tag{4.5}$$

$$\int_o^\infty 4N\pi r^2 e^{-\frac{4N\pi}{3}r^3} dr = 1 \tag{4.6}$$

The modes of the nearest neighbour probability distributions are found from

$$\frac{d^2P}{dr^2} = 0$$

$$\frac{dP}{dr} = y(r) = 4\pi N r^2 e^{-\frac{4N\pi}{3}r^3}$$

and for the modes

$$\frac{d^2P}{dr^2} = \frac{dy}{dr} = 0$$

In which the result is,

$$r_{mode} = \left(\frac{1}{2\pi}\right)^{\frac{1}{3}} \left(\frac{1}{N}\right)^{\frac{1}{3}} \approx 0.54 \left(\frac{1}{N}\right)^{\frac{1}{3}} \tag{4.7}$$

The expectation values of the nearest neighbour seperation,

$$< r > = \int_o^\infty r \left(4\pi N r^2 e^{-\frac{4N\pi}{3}r^3}\right) dr \tag{4.8}$$

$$I = \int 4N\pi r^2 e^{-\frac{4N\pi}{3}r^3} dr = -e^{-\frac{4N\pi}{3}r^3} \tag{4.9}$$

$$< r > \;= rI\Big|_o^{\infty} - \int_o^{\infty} I dr = - \int_o^{\infty} I dr = \int_o^{\infty} e^{-\frac{4N\pi}{3}r^3} dr \tag{4.10}$$

Let

$$a = \frac{4\pi N}{3} \tag{4.11}$$

Substitute into equation 4.10

$$< r >= \int_o^{\infty} e^{-ar^2} dr \tag{4.12}$$

Let u = ar^3, so,

$$\frac{u^{\frac{-2}{3}}}{3a^{\frac{1}{3}}} du = dr \tag{4.13}$$

$$< r > \;= \frac{1}{3a^{\frac{1}{3}}} \int_o^{\infty} u^{-\frac{2}{3}} e^{-u} du = \frac{P(\frac{1}{3})}{3a^{\frac{1}{3}}} \tag{4.14}$$

$$< r > \;= \left(\frac{3}{4\pi}\right)^{\frac{1}{3}} \frac{1}{3} P\left(\frac{1}{3}\right) \left(\frac{1}{N}\right)^{\frac{1}{3}} \approx 0.55 \left(\frac{1}{N}\right)^{\frac{1}{3}} \tag{4.15}$$

The equation used to find the nearest seperation distance is,

$$< r >_{link} = \left(\frac{1}{N}\right)^{\frac{1}{3}} * 0.55 \tag{4.16}$$

.

The redshift range of 0.6 to 2.5 was put into redshift bins of 0.4, in which each bin had their number density calculated, and the linkage scale was calculated for all the bins.

Redshift bin	Distance(h^{-1}Mpc)
0.6 - 1.0	47
0.9 - 1.3	48
1.2 - 1.6	49
1.5 - 1.9	51
1.8 - 2.2	54
2.1 - 2.5	54

TABLE 4.1: Table showing the redshift bins and their calculated linkage scale for stripe 82.

(2) The linkage scale was incorporated into the algorithm for the redshift bin, the algorithm then calculated the distance between each quasar. In the three dimensional case, the use of the simple flat ΛCDM cosmological model in which the Hubble constant depends on redshift z as

$$H^2(z) = H_0^2\Omega_m(1+z)^3[1+(\Omega_\Lambda/\Omega_m)(1+z)^{-3}] \tag{4.17}$$

Where $H_0 = 100h$ km/s Mpc is the present Hubble constant ($h = 0.7$) and $\Omega_m = 0.27$ and $\Omega_\Lambda = 0.73$ which are the cosmological density parameters of matter and dark energy respectively, in units of the critical density. In this model, the comoving line of sight distance is equal to

$$r(z) = \frac{c}{H_0}\int_o^z \frac{dz}{\sqrt{\Omega_m(1+z)^3+\Omega_\Lambda}} = r(z) = \frac{cr_f(z)}{H_0\sqrt{\Omega_m}} \tag{4.18}$$

where,

$$r_f(z) = \int_o^z \frac{dx}{\sqrt{(1+x)^3+\Omega_\Lambda/\Omega_m}} \tag{4.19}$$

Note that when $\Omega = 1$, the comoving distance between two closely located objects is given by the equation

$$dl = \sqrt{dr^2 + r^2(d\theta^2 + sin^2\theta d\phi^2)} \tag{4.20}$$

.

(3) The matching algorithm then selects only those groups which are within the linkage range and have a minimum membership of 8. These groups can then be investigated in 3D to ascertain the morphologies of the groups, through the use of GGobi, a graphical visualization program for exploring high-dimensional data. It provides highly dynamic and interactive graphics such as scatter plot, barchart and parallel coordinates plots. Plots are interactive and linked with brushing and identification, in which 2-D displays of projections of points and edges in high-dimensional spaces, scatterplot matrices, parallel coordinate, time series plots and bar charts. Projection tools include average shifted histograms of single variables, plots of pairs of variables. Points can be labelled and brushed with glyphs and colours. Several displays can be open simultaneously and

linked for labelling and brushing. Missing data are accommodated and their patterns can be examined.

(4) The statistical significance is then tested. The traditional statistical methods in astronomy for assessing clustering and structure (e.g. the 2-point correlation function) are usually unsuitable for finding LQGs and for assessing their significance. In particular, these methods typically have low power for: (i) structure of size $\sim$ survey-size; (ii) directed structures (e.g. filaments); and (iii) isolated, embedded structures. Different methods have been developed for LQGs and have been reasonably effective, but there is still potential for improvements. Graham et al. (1995) adopted a method used in biology, the MST m,σ method, to find their two new LQGs. Tesch & Engels (2000) found their LQG by using a slightly modified form of this method. Komberg et al. (1996) developed a kindred method involving "friends of friends" to find their LQGs.

To test for statistical significance on the groups found, it was necessary to obtain an unbiased estimate of the overdensity by the use of a convex hull approach. The convex hull is defined for any kind of objects made up of points in a vector space, which may have any number of dimensions, including infinite-dimensional vector spaces. The convex hull of finite sets of points and other geometrical objects in a two-dimensional plane or three-dimensional space are special cases of practical importance. The convex hull of a set of points S in n dimensions is the intersection of all convex sets containing S for N points p_1,...p_N. This was created by determining the mean convex hull volume and corresponding density for a set of k points, a random point is then chosen from a selection and its indices of the the k-1 nearest neighbours together with the original point is obtained, the kset points of the convex hull is then computed as well as the convex volume and from this the convex density.

The overdenisty $\Delta\rho/\bar{\rho}$, where $\bar{\rho}$ was obtained by the use of a control field, by using the redshift interval the same as the group found but over a larger area $\sim 400^2$ degrees, the convex hull of the control field was calculated. With the use of the control field and the groups data the overdensity of the groups was found. The identification process was run on simulated stripe-82 catalogue in two categories: (i) RA, Dec and z re-assigned independently by random sampling without replacement; (ii) RA, Dec retained and only z re-assigned by random sampling without replacement. For each category, 1000 simulated catalogues were generated, and analysed for the same magnitude and redshift limits ($1.8 \leq z \leq 2.5$) and ($0.6 \leq z \leq 1.8$). No groups were found in the simulated groups for the selection parameters of all the observed LQGs at a redshift interval of $0.6 \leq z \leq 2.5$. The simulation results show that these groups are real and not a artifact of the algorithm.

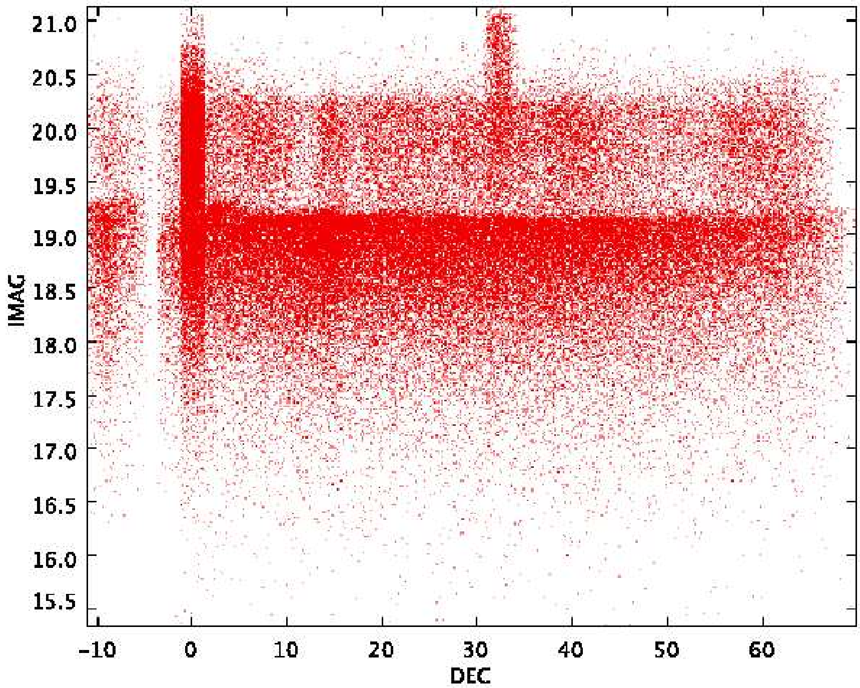

FIGURE 4.1: Showing the non-uniformity of the whole of the SDSS survey with regards to the magnitude

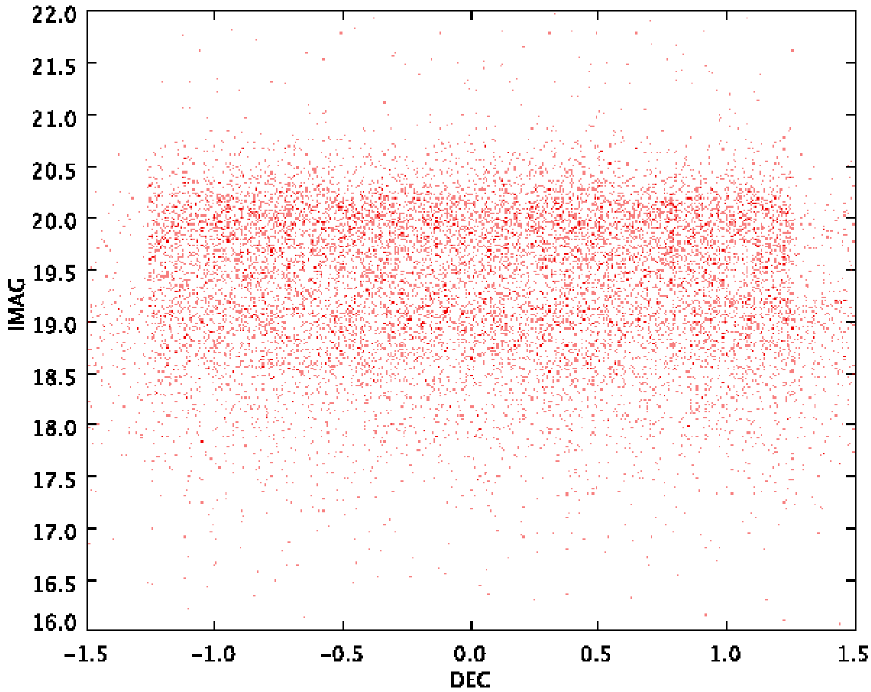

FIGURE 4.2: Plot showing the uniform coverage of stripe 82, with regards to the magnitude

Chapter 5

Results

The database was investigated to find the most uniform area and it was found that the equatorial stripe 82 (RA: $\sim$ 310–60°), across the redshift range 0.6$\leq$ z$\leq$ 2.5, containing 7317 quasars was the most uniform area. It is in this area where the investigation is being done. The search strategy was to use the most common criteria used to describe LQGs, in which the number density must exceed the background density by a factor of two, and the groups should have no fewer than 10 members. I have used the most common criteria for LQGs but have reduced the minimum members to 8. 32 LQGs have been found in the redshift distribution from 0.6 to 2.5. No structures with a minimum membership of 8 members were found below z $\leq$ 0.6, 28 groups have been found between the redshift interval 0.6 to 1.8, with memberships ranging from 8 to 23, and 4 groups found between the redshift interval 1.8 to 2.5 with memberships of 8 to 12. Their morphologies have been investigated and they do appear to have sheet like structure. It does appear that the majority of groups fall in the redshift range of $\sim$ 1.5 of which there are 9. The largest group found with a membership of 23 with a linkage scale of 51 h^{-1} Mpc was found at a redshift of $\sim$ 1.5.

5.1 High redshift LQGs 1.8 to 2.5

Selecting the equatorial stripe 82 (RA: $\sim$ 310–60°) and across the redshift range 1.8–2.4. With a linkage length of 54 h^{-1} Mpc which was calculated from using the nearest neighbour equation, four LQGs have been found, with memberships ranging from 8 to 12, with longest dimensions from 100 to 150 Mpc (proper sizes for the present epoch), and over-densities from $\sim$ 4–8 have been calculated. The two highest redshift LQGs are interestingly close on the sky — $\sim$ 3°, which may suggest that these two groups are one group or maybe joining to create a super group, a more detailed analysis of these two groups is needed. This analysis may be acheived by investigating any gravitational potential between these two groups. The visualization software GGobi has been used to look at the morphologies of these LQGs. And was found that there is a strong impression of sub-clustering or walls in two of the LQGs and a weaker impression in the third. Visualization suggests that the LQG with membership number (12) has two distinct sub-groups separated by $\sim 0.4°$ x $0.4°$, more investigation is required to check the reliability of this finding. The morphologies of the LQGs appear to be sheet like structures. From the search in the equatorial stripe 82 (RA: $\sim$ 310–60°), we have found 4 LQGs, 207 pairs with a minimum linkage length of 6 h^{-1} Mpc, 63 triplets with a minimum linkage length of 11 h^{-1} Mpc

The simulations run on the identified groups found that they are real groups and not artifacts of the algorithm used to find the group's as no group was found in the simulations that were comparable to the identified LQGs. However, the use of simulations can lead to false positives, especially in the choice of linkage length. Increasing the linkage length will increase the probability of false positive detections. When using an algorithmic approach to identify LQGs, it is nessacary to employ some criterion in order to identify if the the group found is real. A theoretical approach is to see if the group is gravitationally bound or if the groups properties are similar to those of real structures (Nadathur 2013).

Name	No	RA(J2000)	Dec(J2000)	z	nnsep h^{-1}Mpc	density h^3Mpc^{-3}	overdensity
LQG 1	9	38	0.3	2.03	29.39	7.70e-05	4.90
LQG 2	12	41	-0.4	2.12	30.68	6.04e-05	8.22
LQG 3	11	344	-0.3	1.98	34.20	3.79e-05	7.24
LQG 4	8	354	0.1	1.89	30.22	9.72e-05	6.04

Table 5.1: Table showing the four groups found at the redshift interval of 1.8 to 2.5, showing the centre of the groups the mean z, mean nearest neighbour separation (h^{-1} Mpc), density and the overdensity

LQGs at the redshift interval of 0.6 to 1.8

The investigation then took the redshift distribution of 0.0 to 1.8 of the equatorial stripe 82 (RA: $\sim$ 310–60°) and searched for LQGs, in redshift intervals of 0.4 with each linkage length being calculated for the redshift interval. The total number of groups found is 28, with the groups ranging in memberships from 8 to 23, below $z \leq 0.6$ no groups where found with a minimum member of 8. See table 5.2 for details of the groups found.

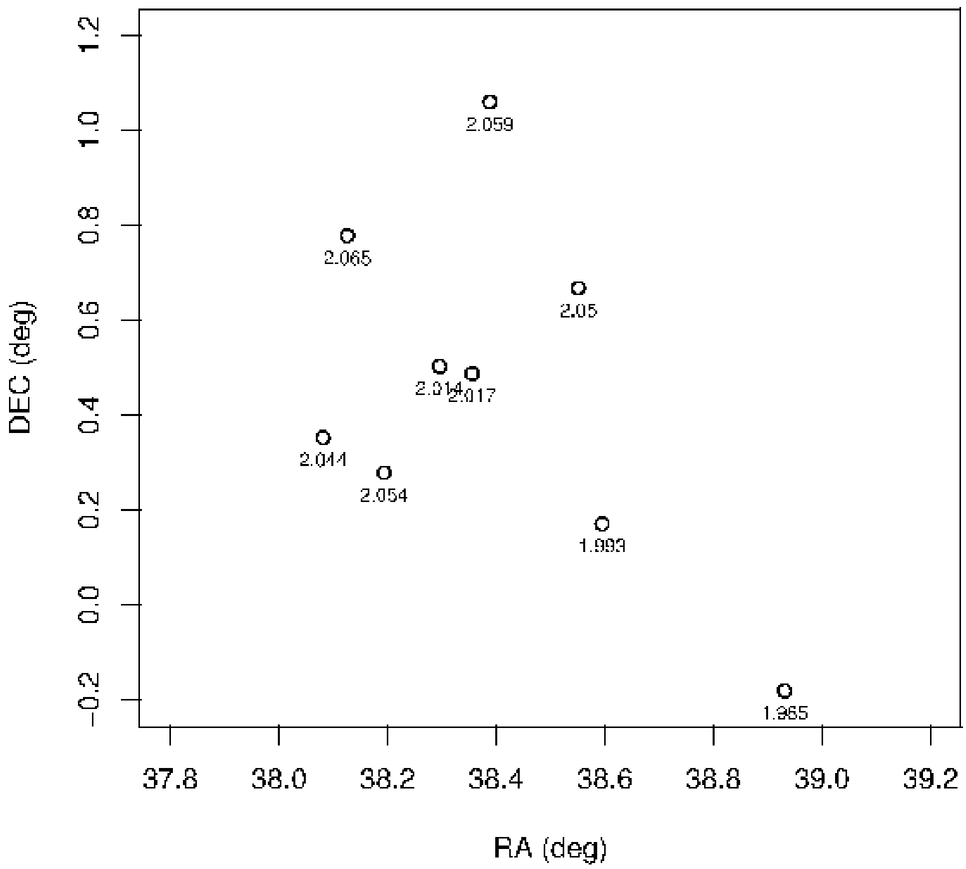

FIGURE 5.1: Plot of LQG 1, with 9 members and a redshift interval of 1.985 to 2.065

5.2 Summary

The distribution of these groups, suggests that there is no preferred redshift for the groups to form, as there is a group of 23 at z $\sim$ 1.5 and a group of 12 at z $\sim$ 2. As we can see from the redshift distribution the 2 largest groups are found to be at a redshift interval of $\sim$ 1.5 - 2.1.

If we compare this with the histogram of the database with a redshift range of 0.0 - 5.4 , the peak of quasar occurrence has been suggested to lie in the redshift interval of $\sim$ 1.5 -2.0 See Figure 5.5. The plotted histogram Figure 5.6 shows at what redshift the majority of the LQGs fall, the peak of the group occurrence is $\sim$ 1.5. Which is the same for the peak occurrence for the quasar distribution, which gives more evidence that the redshift $\sim$ 1.5 will be the best place to look for LQGs.

During the search for high redshift LQGs, many pairs and triplets were found, but interestingly they are mainly found in the redshift interval 1.8 - 1.9, with a sharp decrease in numbers as the redshift increased.

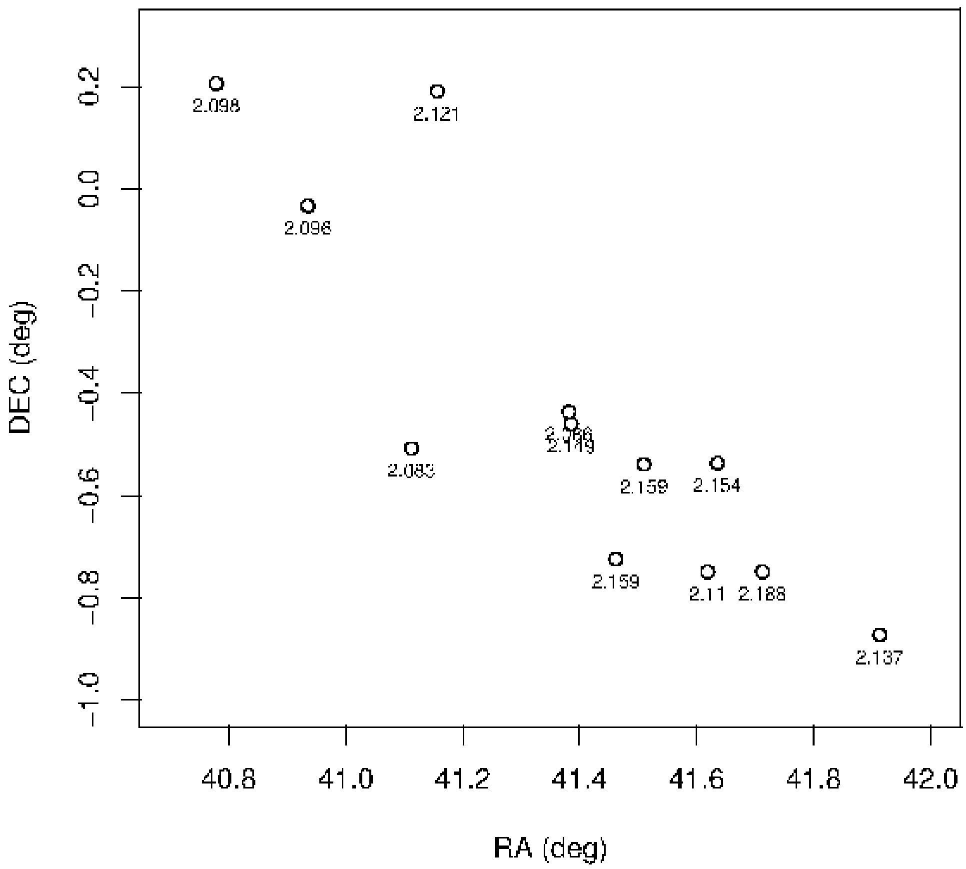

FIGURE 5.2: Plot of LQG 2 with 12 members and a redshift interval of 2.083 to 2.188

The two areas analyzed by Pilipenko (2007), were also investigated for LQGs. But due to the non-uniformity of these two areas, the magnitude i was constrained to the range of ≤ 19.1, which in turn reduces the amount of quasars available. The calculated nearest neighbour distances was found to be $\sim$100 h^{-1}Mpc which may be an unrealistic distance to use, but Clowes (2007), suggests an indication of layered sub-structure, which would require a greater nearest neighbour distance to reveal this layered sub-structure, more investigation is required to establish the association.

I therefore used the linkage length of 54h^{-1}Mpc but found no group larger than 6 members, which confirms Pilipenko$'$s results. Pilipenko (2007) suggests that quasars tend to lie in large scale sheets, from my examination of the groups through the use of GGobi they do appear to lie in sheets, but more work is needed to establish the details of the association.

See appendix for complete list of coordinates and redshift for all members of the groups.

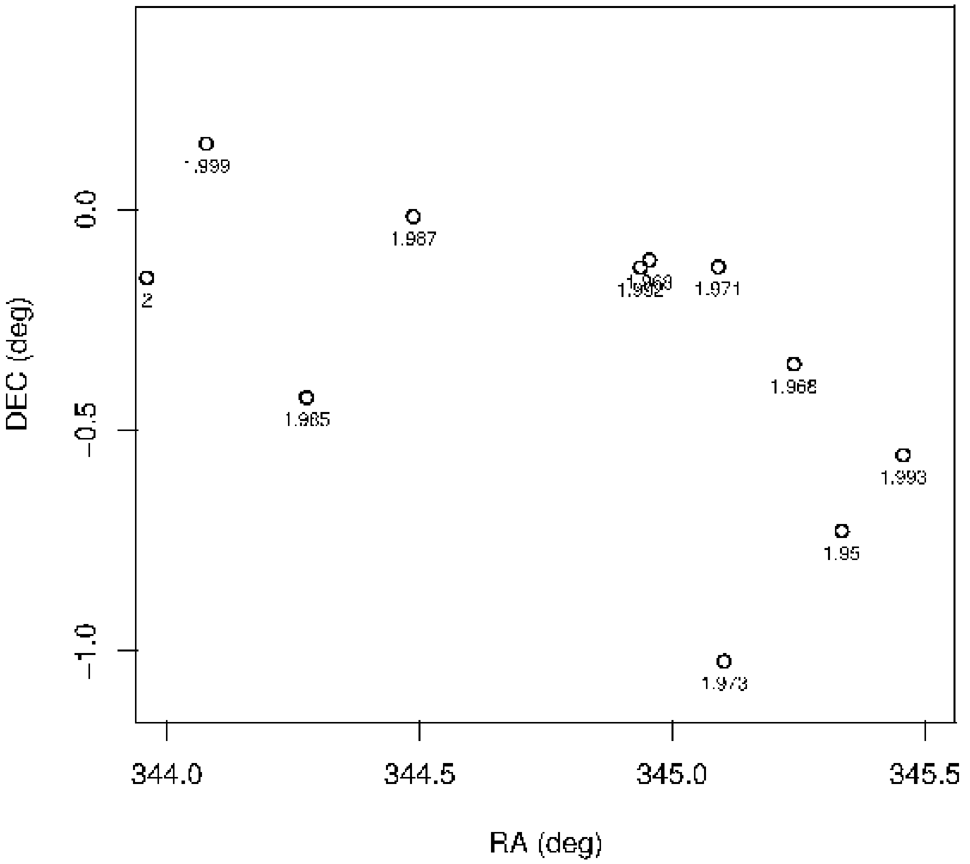

FIGURE 5.3: Plot of LQG 3 with 11 members and a redshift interval of 1.871 to 2.0

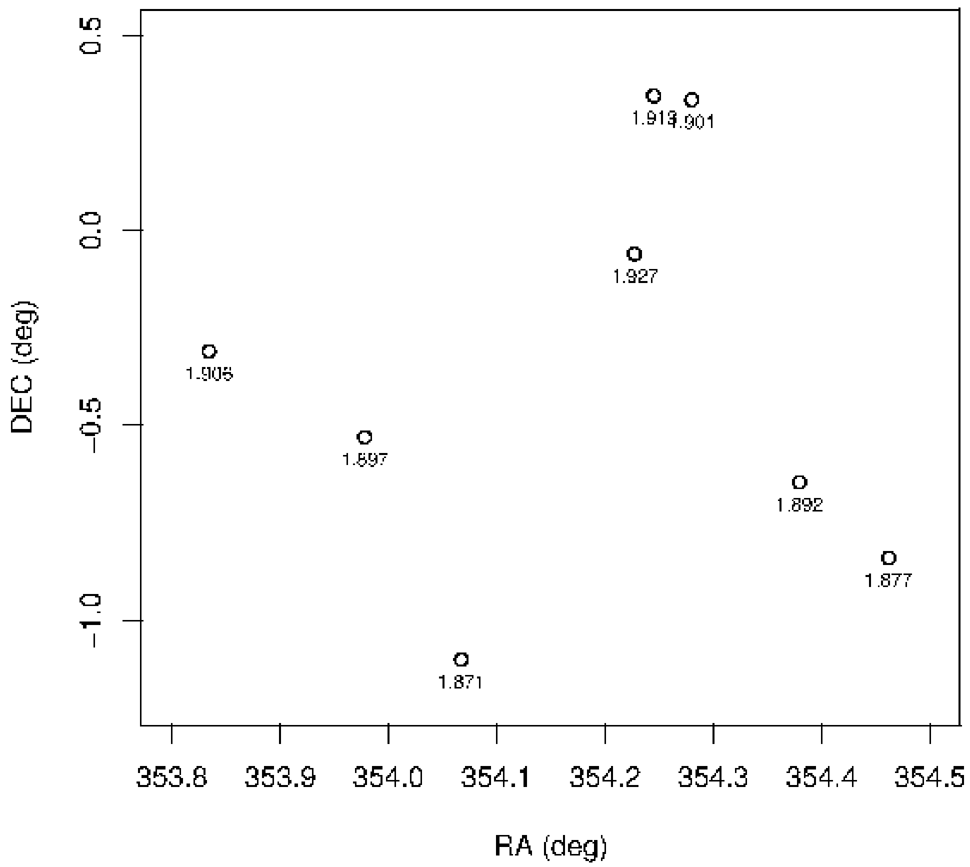

FIGURE 5.4: Plot of LQG 4 with 8 members with a redshift interval of 1.871 to 1.927

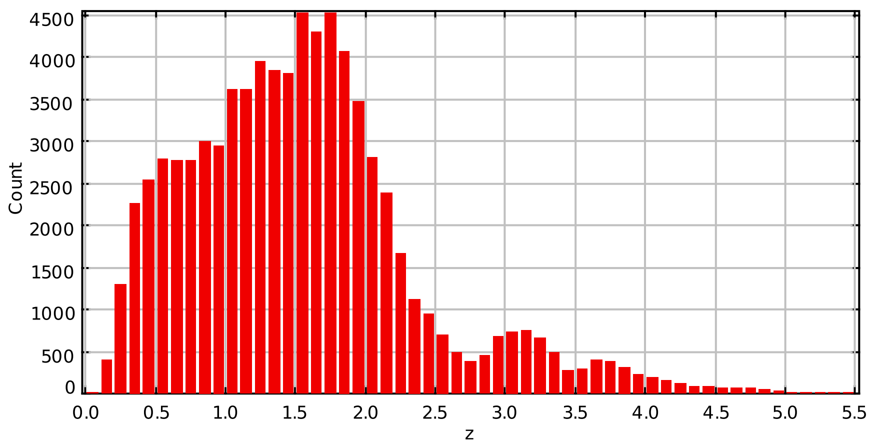

FIGURE 5.5: A histogram showing the redshifts of all quasars in the SDSS DR7, which suggests that the peak occurrence can be seen to lie within the redshift interval 1.5 to 2.0

Name	No	RA(J2000)	Dec(J2000)	z	nnsep h^{-1}Mpc	density h^3Mpc^{-3}	overdensity
LQG 5	13	40.4	0.5	1.07	23	9.47e-05	6.78
LQG 6	8	35	-0.4	1.17	34	1.13e-04	3.73
LQG 7	9	35.4	-0.5	1.04	26	1.70e-04	5.10
LQG 8	10	1.5	0.0	1.03	26	2.19e-04	7.45
LQG 9	8	41.5	0.4	0.64	25	2.08e-04	3.79
LQG 10	11	37	0.0	0.61	27	8.77e-05	2.98
LQG 11	11	15.1	0.0	0.74	23	1.14e-04	4.05
LQG 12	8	11.5	0.4	0.82	22	1.21e-04	3.06
LQG 13	10	355	0.0	0.71	18	2.07e-04	6.6
LQG 14	10	352	-0.5	0.62	36	8.85e-05	3.2
LQG 15	8	333	-0.2	0.75	31	1.28e-04	5.90
LQG 16	9	313	0.1	0.68	26	1.60e-04	6.94
LQG 17	10	356	0.5	1.25	32	5.28e-05	6.1
LQG 18	8	22	-0.7	1.75	31	9.74e-05	6.6
LQG 19	10	47	-0.6	1.42	34	5.93e-05	6
LQG 20	11	28	0.5	1.39	36	4.67e-05	4
LQG 21	23	35	-0.6	1.55	32	1.61e-05	4
LQG 22	9	12	0.5	1.58	27	1.08e-04	4.5
LQG 23	13	50	0.5	1.78	35	3.20e-05	4
LQG 24	12	52	0.5	1.52	29	4.99e-05	6
LQG 25	10	17	0.1	1.76	29	8.41e-05	6.5
LQG 26	8	50	-0.8	1.56	25	1.42e-04	5
LQG 27	12	8	0.1	1.71	33	5.26e-05	4.5
LQG 28	9	52	0.6	1.77	24	8.12e-05	5
LQG 29	15	18	-0.5	1.55	35	3.52e-05	3.5
LQG 30	10	356	0.5	1.25	32	5.28e-05	5
LQG 31	8	330	0.4	1.56	28	1.20e-04	5
LQG 32	8	331	-0.7	1.52	32	9.47e-05	4

Table 5.2: Table showing the groups found at the redshift interval of 0.6 to 1.8, showing the centre of the groups the mean z, mean nearest neighbour separation (h^{-1} Mpc), density and the overdensity

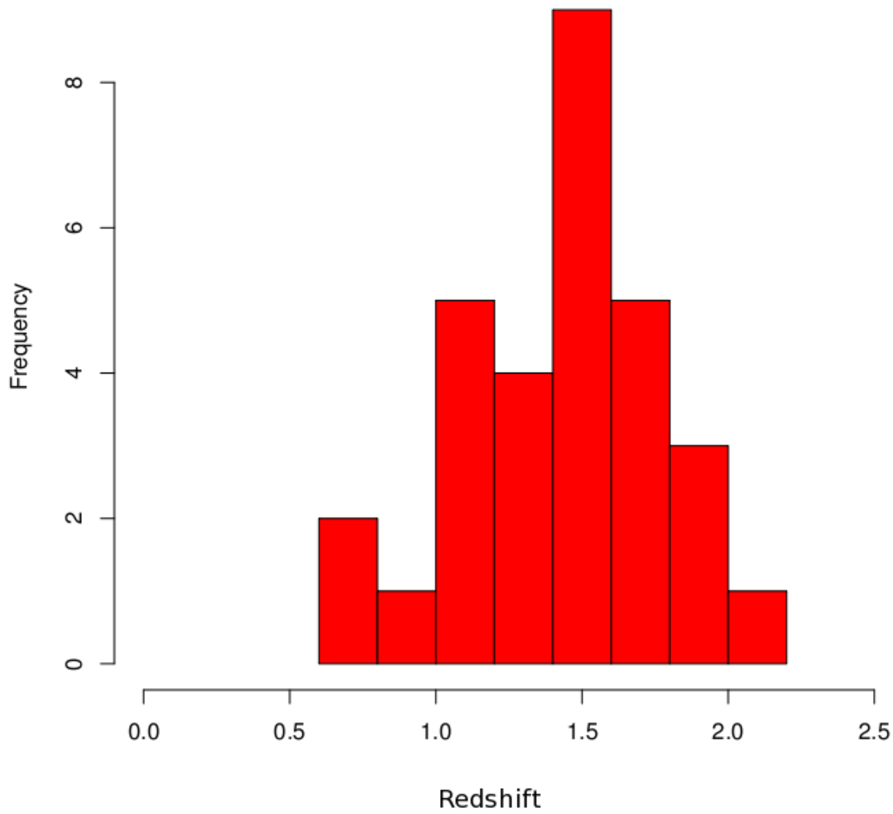

Figure 5.6: A histogram showing the frequency of the LQGs, with respect to the redshift of the groups.

Chapter 6

MgII Absorbers

The relative overdenisty of forms of matter in LQGs is not well determined. Doroshkevich et al. (1999) found from simulations, that from the present epoch to z $\sim$ 4, the density drops for the matter accumulated by the largest wall like structures by a factor of $\sim$ 4 and becomes negligible by z = 3. They suggested that any detailed statistical investigations of super large-scale structures will require quasar absorbers at such epochs. The advantages of the absorbers is that they are able to trace much lower overdenities than quasars themselves. A significant excess of MgII absorbers compared with published data from non-LQG fields (Mshar et al. 2007, Steidel & Sargent 1992) will show that the enhancement in the density of quasars is indeed associated with a corresponding general enhancement of the mass (galaxies). This approach has been used before, by Williger et al. (2002), where it provided an independent confirmation of the Clowes & Campusano(1995) LQG at z $\sim$ 1.3. In that case the MgII absorbers showed an enhancement of $\sim$ 100. Furthermore, the combination of MgII absorbers and known quasars led to the discovery of a previously unrecognised LQG at z $\sim$ 0.8. For the present epoch, Einasto et al. (2008) note, however, that the occurrence in the simulations of rich superclusters is much lower than is actually observed.

There is currently rather little work upon which to draw for the theoretical expectations for the observational properties of large-scale structure at high redshifts. Doroshkevich et al. (1999) used N-body simulations to investigate what they called "rich structure elements" - RSEs. These RSEs are wall-like structures with sizes $\sim 70h^{-1}$ Mpc that contain $\sim$ 40% of the mass (dark matter) at the present epoch. Doroshkevich et al. say that at z $\sim$ 1 the fraction of the mass in the RSEs is $\sim$ 20%, and that at z $\sim$ 3 it is negligible, but no fraction is given for z $\sim$ 2. The MgII absorbers will allow us to estimate directly the fraction of the mass that is contained in LQGs at z $\sim$ 2.

Given that the MgII absorbers are likely to demonstrate that the quasar enhancements of the LQGs are associated with corresponding mass enhancements, these four z $\sim$ 2 LQGs should be prime sites for the identification of high-z clusters. Several papers have shown that, in projection at least, quasars tend to lie on the peripheries of clusters rather than be embedded within them (e.g. Soechting et al. 2002, 2004; Tanaka et al. 2001; Haines et al. 2001; Sanchez & Gonzalez-Serrano 1999). Individual clusters of galaxies within the LQGs are then not likely to be centred on the member quasars. However, the positions of the MgII absorbers are likely to be productive sites for finding high z clusters in subsequent observations.

6.1 Gemini

The Gemini Observatory consists of two 8.1 meter diameter, altitude - azimuth mounted telescopes, the Gemini South telescope on the summit of Cerro Pachon in Chile and the Frederick C. Gillett Gemini North telescope on the summit of Mauna Kea on the island of Hawaii. To investigate the LQGs the use of the MgII 2796, 2803 doublet of absorbers in the background quasars will be appearing in the range $\sim$ 8100-8750Å. Which a spectra resolution of $\sim$ 2Å, in the rest frame of the LQGs, which translates to $\sim$ 6Åin instrumental resolution. This is achieved by using an R400 grating with 0.75" slit, the significant spectra coverage of the grating (4000Å) will allow detection of MgII absorbers within a large redshift range typically 1<z<2.4 improving the statistical findings of the LQGs. However, the data recived by Gemini held no relevant information to use, this is primarily due to the time of use of the Gemini,bad weather and low visabilty have lead to having data to use.

6.2 Zhu & Maynard Catalogue

Zhu & Maynard (2012), created a catalogue, using a fully automated method aimed at detecting absorption lines in the spectra of astronomical objects. This algorithm estimates the source continuum flux by using a dimensionality reduction technigue, nonnegative matrix factorization, which then detects and identifies the metal absorption lines. From their investigation they find that, the rest equivalent width distribution of strong Mg II absorbers follows an exponential distribution at all redshifts, which confirms previous studies. They also find that the redshift evolution of strong Mg II aborbers to be similar to that of the cosmic star formation history over $0.4 < z < 5.5$, in which this suggests a possible physical link between these two quantities. They created this catalog with the use of the SDSS DR7 catalog, using the redshift estimates provided by Hewett & Wild (2010), which also includes 1411 visually inspected quasars.

6.3 Results

The Gemini data was collected and reduced using IRAF code. The procedure for reducing the Gemini data is as follows. Bias images were created using gbias. The flat fields were made and combined by using gsflat and gscut, the science data was reduced, in which the bias was subtracted, the data was cleaned of cosmic rays, the flat-comb frame that was created with gsflat was updated with the location of the slit edges, the spectra was then reduced. The CuAr spectrum was reduced but not flat fielded. The wavelength calibration was then established, and the transform of the CuAr spectrum was done and each of the SCI extensions was inspected. The science exposures are then transformed and the sky was subracted from the science exposures, where each of the SCI extensions of the sky subtracted spectra was inspected. Gextract was then used to extract all the spectra and each spectra was inspected. However, the Gemini data after the reduction was found to hold no relevant information, this may be a cause from time of exposure and weather at the time of exposure, and as such no information came from the reduced data.

Using the structure finding algorithim on the Zhu & Menard catalogue (2012), first to find any Mg II groups with minimum membership of 8, within a redshift interval of 1.8 - 2.8. However, no group larger than triplets were found. The investigation then looked at if any Mg II absorbers were found near the LQGs. Preliminary findings from this catalogue have found, LQG 1 has 12 Mg II absorbers close to the group with one of the quasars in the group being very close to an absorber. LQG 2 has 13 Mg II absorbers close to the group, with 4 absorbers being very close to 4 quasars. LQG 3 has 16 absorbers around the group. LQG 4 has 9 absorbers around the group, but no absorbers in the group. These Mg II absorbers do appear to lie on the peripherals of the groups, which is consistent with current investigations. These results are still in need of further validation to confirm the results.

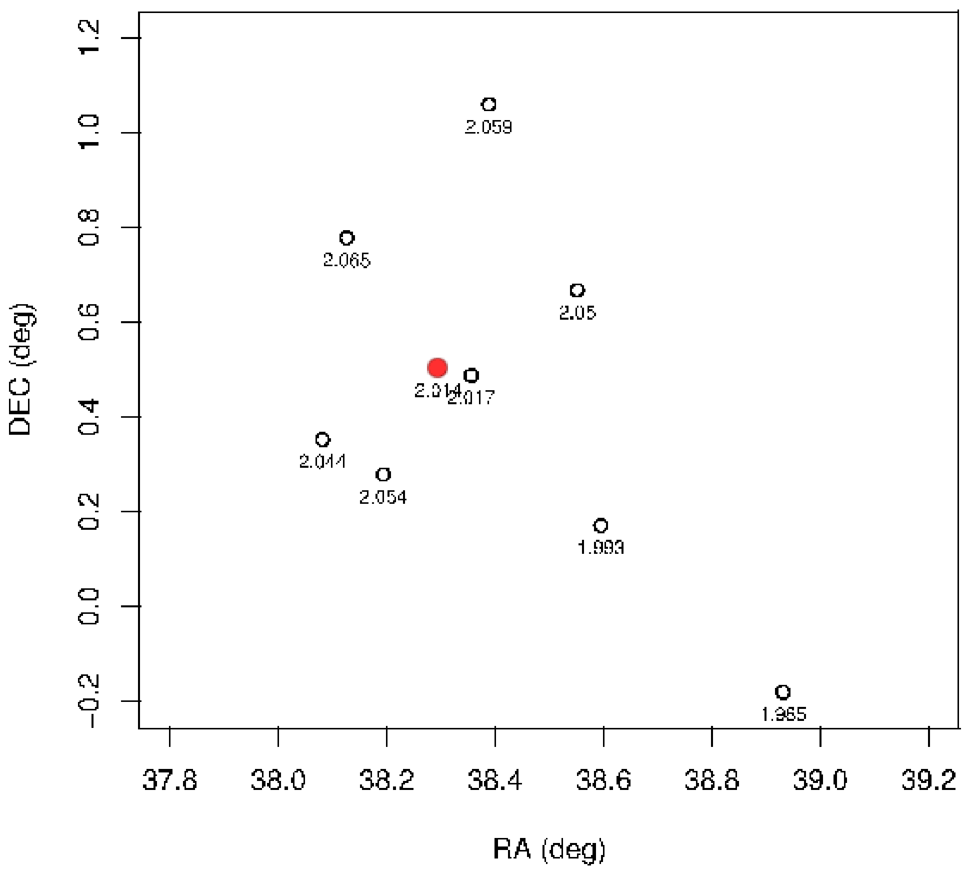

FIGURE 6.1: Plot of LQG 1 and the Mg II Absorbers found within the redshift range of the LQG, the absorbers are in red

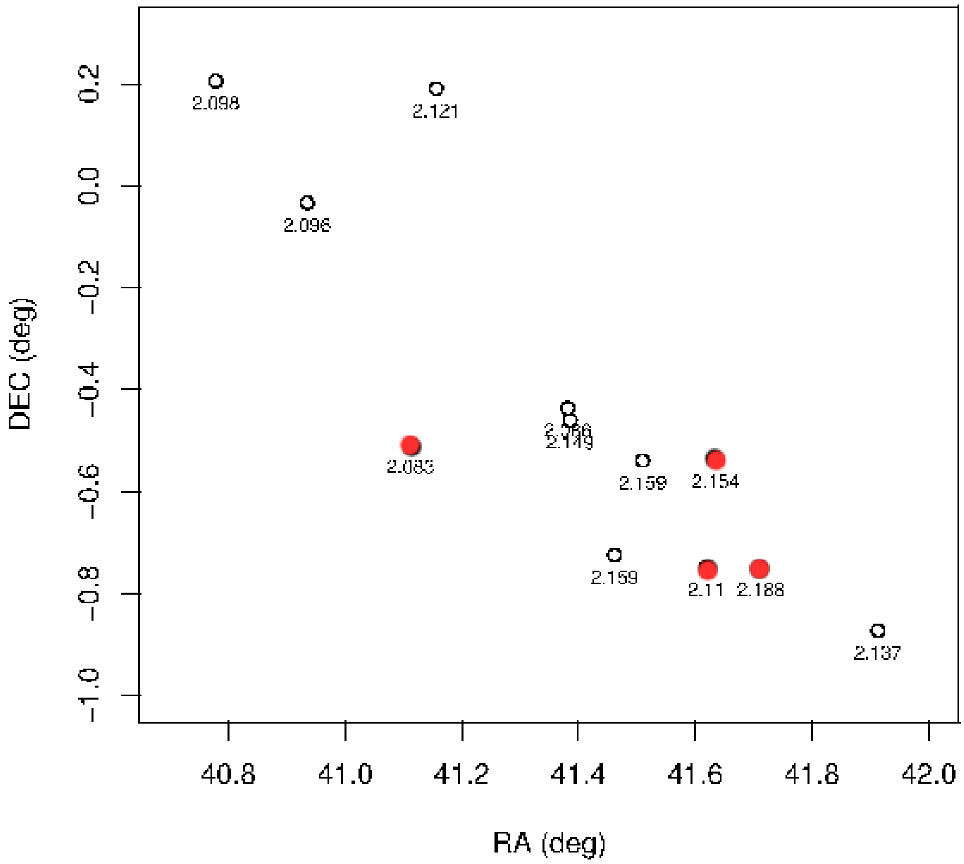

FIGURE 6.2: Plot of LQG 2 and the Mg II Absorbers found within the redshift range of the LQG, the absorbers are in red

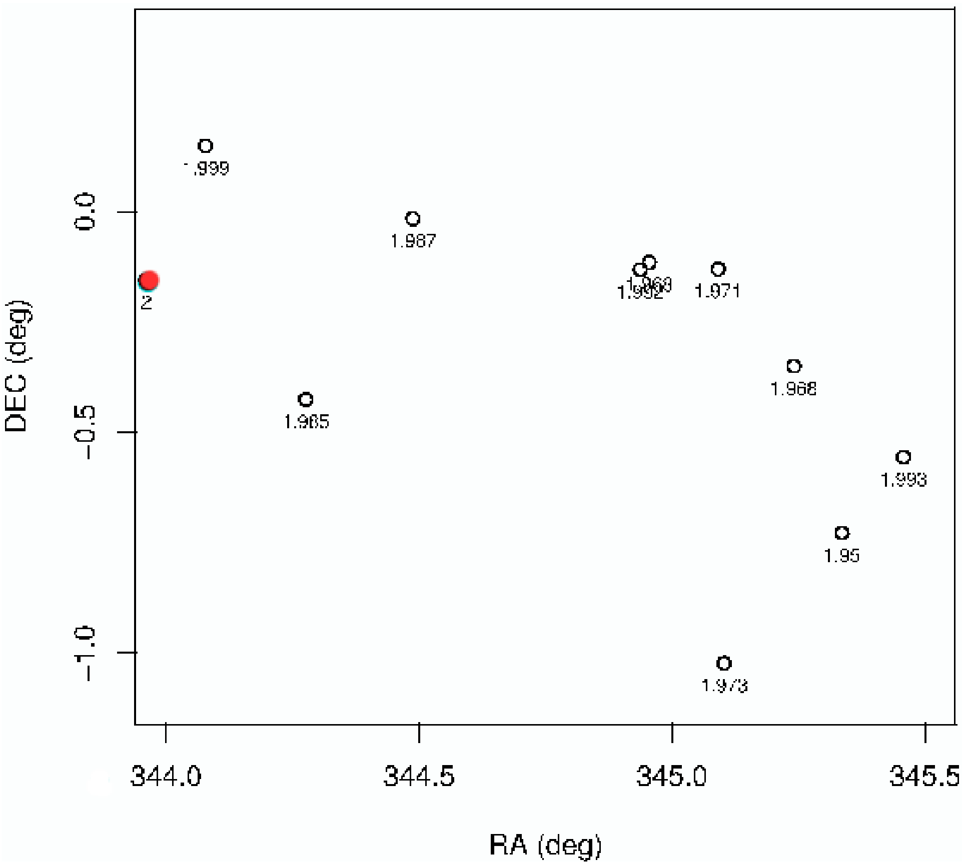

FIGURE 6.3: Plot of LQG 3 and the Mg II Absorbers found within the redshift range of the LQG, the absorbers are in red

Chapter 7

Future Work

7.1 Aims

The main aim of this work is to determine the properties of LQGs - redshift , physical size, morphology, membership, luminosity range of members. To assess the selection effects and the compatibilty of the LQGs with the concordance model in cosmology. The detection of low to intermediate redshift LQGs will allow for the studying of cluster enviroments that favor the formation of quasars; the mechanisms of quasar formation; the properties of the largest large scale structures and the relation of quasars to mass. The development of a second algorithm to find LQGs, based on gravitational potential and apply this method to the groups already found and stripe 82.

Using two methods of finding LQGs in conjunction to produce a final sample of LQGs that has greater completeness than would be possible with a single method. The selection effects of both methods can be assessed, to continue to develop a procedure to test their statistical significance. Once completed a catalog will be created of the identified LQGs, their properties will be investigated, and the variation of these properties with redshift, in which it may be possible to disscuss whether there is a cut-off redshift.

Given that the MgII absorbers are likely to demonstrate that the quasar enhancements of the LQGs are associated with corresponding mass enhancements, these LQGs should be prime sites for the identification of high-z clusters. Several papers have shown that, in projection at least, quasars tend to lie on the peripheries of clusters rather than be embedded within them (e.g. Soechting et al. 2002, 2004; Tanaka et al. 2001; Haines et al. 2001; Sanchez Gonzalez-Serrano 1999). Individual clusters of galaxies within the LQGs are then not likely to be centred on the member quasars. However, the positions of the MgII absorbers are likely to be productive sites for finding high-z clusters in subsequent observations.

Analysis of the degree of clustering with redshift can be compared with the predictions of linear theory. Not much is known about the expectation of LQGs at high redshift, in which information is sparse on the theoretical expectations for detecting large-scale structures at $z \sim 2$, even though the simulations of Einasto et al. (2008) have suggested that few clusters would be found at such redshifts. Using the results found from investigating the LQGs, it will be possible to investigate the expectation of finding LQGs at high redshift, and therefore be able to put constraints on acceptable choices of cosmological model.

Appendix A

Tables of Results of the full list of quasars found

RA	Dec	z	i	M_i
02:32:19.52	+00:21:06.8	2.044	18.983	-26.484
02:32:30.21	+00:46:39.6	2.064	20.661	-24.822
02:32:46.48	+00:16:42.6	2.054	19.556	-25.924
02:33:10.93	+00:30:08.1	2.013	20.28	-25.148
02:33:25.32	+00:29:14.8	2.017	18.304	-27.129
02:33:33.23	+01:03:33.0	2.058	18.346	-27.128
02:34:12.34	+00:40:02.9	2.049	19.885	-25.578
02:34:22.85	+00:10:14.2	1.992	20.188	-25.213
02:35:43.36	-00:10:51.4	1.985	20.076	-25.323
02:43:06.83	+00:12:19.4	2.097	19.247	-26.287
02:43:44.31	-00:02:01.0	2.096	19.560	-25.967
02:44:26.88	-00:30:28.4	2.087	20.160	-25.365
02:44:37.49	+00:11:25.2	2.109	19.712	-25.846
02:45:31.53	-00:26:12.2	2.085	19.823	-25.699
02:45:32.49	-00:27:37.9	2.148	20.098	-25.494
02:45:50.79	-00:43:28.1	2.158	20.177	-25.423
02:46:02.34	-00:32:21.5	2.159	20.132	-25.478
02:46:28.49	-00:44:57.1	2.110	19.749	-25.801
02:46:32.44	-00:32:14.2	2.153	18.501	-27.102
02:46:50.93	-00:44:57.3	2.187	19.028	-26.613
02:47:39.11	-00:52:21.1	2.136	20.229	-25.376
23:35:20.21	-00:18:34.1	1.906	19.610	-25.716
23:35:54.72	-00:31:48.6	1.897	19.989	-25.331
23:36:16.09	-01:06:03.5	1.871	19.372	-25.903
23:36:54.51	-00:03:36.1	1.926	19.977	-25.369
23:36:58.76	+00:20:44.4	1.913	19.807	-25.53
23:37:07.23	+00:20:06.8	1.900	19.108	-26.215
23:37:31.02	-00:38:47.1	1.891	19.962	-25.341
23:37:50.82	-00:50:23.0	1.877	19.572	-25.709

TABLE A.1: Table showing the position, redshift and magnitude of each quasar in the LQGs

RA	Dec	z	i	M_i
22:55:50.40	-00:09:17.7	1.999	19.974	-25.534
22:56:18.65	+00:08:55.6	1.999	19.596	-25.893
22:57:06.17	-00:25:32.8	1.985	18.535	-26.93
22:57:56.99	-00:00:58.9	1.987	19.030	-26.439
22:59:44.89	-00:07:53.0	1.992	19.991	-25.473
22:59:49.11	-00:06:54.3	1.967	18.497	-26.941
23:00:21.83	-00:07:49.0	1.971	19.061	-26.379
23:00:24.59	-01:01:22.3	1.973	19.471	-25.958
23:00:57.67	-00:21:02.5	1.968	19.322	-26.112
23:01:20.47	-00:43:41.8	1.949	19.432	-25.982
23:01:49.68	-00:33:22.1	1.992	20.282	-25.187
00:42:28.38	+01:08:44.6	0.8162	19.612	-23.661
00:43:38.28	+00:05:23.8	0.8215	19.045	-24.24
00:43:41.24	+00:52:53.3	0.8344	18.707	-24.624
00:43:41.48	+00:56:10.0	0.8300	19.551	-23.768
00:43:51.41	+00:09:56.8	0.8234	20.101	-23.19
00:46:10.17	+00:04:49.7	0.8242	19.197	-24.097
00:49:19.68	-00:10:31.5	0.8170	19.780	-23.518
00:51:28.91	+00:08:52.9	0.8209	20.493	-22.799
02:41:41.52	+00:04:16.6	0.6485	18.728	-24.006
02:42:27.34	+00:08:45.4	0.6500	20.630	-22.125
02:42:40.96	+00:21:50.8	0.6327	20.039	-22.636
02:43:36.94	+00:31:33.1	0.6264	19.849	-22.812
02:45:33.66	-00:07:45.0	0.6539	19.008	-23.748
02:45:35.92	+00:05:37.8	0.6400	19.315	-23.389
02:47:05.67	+00:18:34.5	0.6501	19.314	-23.44
02:49:48.62	+00:51:52.9	0.6583	20.185	-22.646

Table A.2: Table showing the position, redshift and magnitude of each quasar in the LQGs

RA	Dec	z	i	M_i
03:16:47.56	-00:15:39.7	0.9046	19.951	-23.684
03:17:30.04	+00:00:52.6	0.8919	20.472	-21.375
03:19:10.24	+00:07:27.1	0.8771	20.314	-23.249
03:19:10.66	-00:02:33.7	0.8671	19.435	-24.109
03:20:14.39	+00:48:25.5	0.8612	20.348	-23.271
03:20:17.86	+00:06:47.8	0.8830	19.352	-24.245
03:20:38.93	+00:25:11.2	0.8762	20.723	-22.884
03:21:19.78	+01:11:05.8	0.8552	20.681	-22.905
00:59:05.50	+00:06:51.6	0.7189	17.514	-25.465
00:59:23.89	-00:01:20.4	0.7470	20.193	-22.876
00:59:50.35	+00:29:38.0	0.7479	19.325	-23.756
01:00:02.05	+00:47:33.5	0.7207	19.501	-23.479
01:00:02.32	+00:16:42.5	0.7771	17.472	-25.708
01:00:07.28	-00:32:18.5	0.7358	19.722	-23.322
01:00:33.50	+00:22:00.1	0.7535	18.118	-24.981
01:00:47.68	-00:37:52.2	0.7331	18.882	-24.157
01:00:49.93	+00:25:54.1	0.7569	20.076	-23.028
01:01:16.63	+00:04:48.4	0.7683	19.762	-23.389
01:02:05.89	+00:11:56.9	0.7253	17.088	-25.928
02:22:29.99	+00:48:37.5	0.6152	19.617	-23.002
02:26:04.15	+01:08:03.1	0.6162	19.652	-22.964
02:26:14.46	+00:15:29.7	0.6151	16.943	-25.68
02:26:52.23	-00:39:16.4	0.6252	19.943	-22.704
02:27:21.25	-01:04:45.8	0.6147	19.900	-22.714
02:28:37.85	+00:22:15.4	0.6182	19.908	-22.706
02:29:30.91	-00:08:45.3	0.6089	19.076	-23.494
02:31:28.98	+01:12:50.1	0.6013	20.052	-22.487
02:33:18.76	+00:21:25.7	0.6090	19.897	-22.676
02:33:30.95	+00:12:06.8	0.6058	19.426	-23.137
02:33:36.09	+00:30:14.4	0.6091	19.782	-22.792

TABLE A.3: Table showing the position, redshift and magnitude of each quasar in the LQGs

RA	Dec	z	i	M_i
02:17:35.44	+00:14:56.2	1.1693	20.053	-24.126
02:17:52.75	+00:15:21.6	1.1727	19.626	-24.564
02:18:40.53	-00:15:16.0	1.1714	18.946	-25.232
02:19:40.41	-00:28:21.0	1.1567	19.896	-24.251
02:19:53.28	-01:00:25.2	1.1919	19.471	-24.744
02:20:08.24	-00:06:58.8	1.1871	19.979	-24.234
02:20:56.02	-00:51:37.0	1.1683	19.532	-24.634
02:21:57.84	-00:34:15.8	1.1963	19.953	-24.271
02:19:51.74	-00:44:35.2	1.0348	19.281	-24.599
02:19:58.68	-00:09:42.4	1.0217	20.081	-23.769
02:21:39.18	-00:21:47.6	1.0463	19.511	-24.399
02:21:53.52	-00:10:14.8	1.0469	19.808	-24.100
02:21:57.81	+00:00:42.5	1.0418	18.537	-25.369
02:21:58.77	-00:10:44.4	1.0381	19.960	-23.929
02:22:12.43	-01:03:04.6	1.0259	19.131	-24.728
02:22:14.56	-00:03:21.8	1.0662	19.298	-24.660
02:22:22.80	-00:07:45.6	1.0552	20.091	-23.839
00:03:55.49	+00:07:36.4	1.0274	19.555	-24.292
00:04:51.86	-00:12:03.7	1.0278	19.413	-24.711
00:04:56.17	+00:06:45.5	1.0412	19.688	-24.194
00:05:20.99	-00:19:48.3	1.0423	20.207	-23.684
00:05:25.12	+00:17:45.2	1.0285	19.511	-24.383
00:05:30.14	-00:23:56.2	1.0605	20.077	-23.861
00:06:10.07	+00:25:59.8	1.0264	19.990	-23.929
00:06:22.60	-00:04:24.4	1.0381	19.580	-24.328
00:06:45.41	+00:06:13.9	1.0308	19.827	-24.080
00:08:12.29	+00:13:12.4	1.0510	19.531	-24.449
02:39:57.24	+01:15:36.2	1.0750	19.931	-24.044
02:40:03.99	+00:25:38.6	1.1027	20.013	-24.010
02:40:46.85	-00:13:24.9	1.1015	20.253	-23.116
02:41:02.27	+00:50:33.7	1.0852	20.242	-23.760
02:41:04.28	+00:08:21.2	1.0575	19.518	-24.402
02:41:18.35	+00:29:29.0	1.0934	19.968	-24.044
02:41:22.43	-00:00:07.3	1.0694	19.827	-24.117
02:41:32.08	-00:08:20.2	1.1060	19.829	-24.193
02:41:45.19	+00:30:28.4	1.0508	19.806	-24.107
02:41:56.15	+00:34:41.7	1.0508	18.740	-25.171
02:42:00.91	+00:00:21.0	1.1041	18.502	-25.524
02:42:41.94	+00:37:30.6	1.0616	20.337	-23.597
02:43:00.72	+00:41:58.1	1.0768	20.707	-23.259

TABLE A.4: Table showing the position, redshift and magnitude of each quasar in the LQGs

RA	Dec	z	i	M_i
00:45:05.54	+00:31:42.7	1.5397	20.155	-24.639
00:45:16.00	+00:00:42.3	1.5519	18.479	-26.322
00:45:25.11	-00:34:33.9	1.5503	19.783	-25.021
00:45:55.82	+00:54:55.1	1.5503	19.837	-24.978
00:46:26.37	+00:13:15.7	1.5417	18.719	-26.080
00:47:46.24	-00:00:36.4	1.5410	19.028	-25.776
00:47:59.36	+00:15:50.5	1.5610	19.819	-25.004
00:48:19.12	+00:14:57.1	1.5452	19.731	-25.069
03:17:32.68	-00:55:13.4	1.5591	20.775	-24.116
03:18:44.33	-00:36:05.1	1.5668	20.116	-24.808
03:19:26.24	-00:28:44.8	1.5730	20.279	-24.658
03:20:29.37	-01:03:01.4	1.5678	19.740	-25.194
03:20:31.70	-00:51:30.2	1.5780	20.087	-24.860
03:21:22.35	-01:06:00.4	1.5693	18.688	-26.272
03:23:24.30	-00:58:54.7	1.5699	18.788	-26.198
03:24:05.19	-01:01:40.5	1.5534	20.260	-24.737
00:14:34.13	+00:29:57.1	1.3450	20.181	-24.306
00:15:26.52	+00:18:13.2	1.3620	19.529	-24.985
00:15:35.54	+00:53:56.0	1.3587	18.941	-25.570
00:15:36.78	+00:37:57.3	1.3722	20.311	-24.221
00:15:59.58	+00:42:12.9	1.3358	19.680	-24.787
00:18:04.32	+01:00:31.4	1.3440	19.670	-24.822
00:19:16.91	+00:47:07.9	1.3156	19.986	-24.450
00:20:19.68	+00:58:22.0	1.3359	19.597	-24.450
00:21:30.66	+00:55:27.3	1.3330	19.610	-24.847
02:47:53.20	-00:21:37.8	1.4381	19.803	-24.880
02:48:20.91	-00:25:46.8	1.4547	19.361	-25.347
02:48:47.27	-00:13:09.5	1.4428	18.542	-26.162
02:49:29.18	-00:21:04.2	1.4298	18.479	-26.210
02:49:35.55	-00:13:36.8	1.4191	19.490	-25.185
02:50:30.77	-00:08:01.8	1.4601	17.870	-26.890
02:51:02.69	+00:06:00.6	1.4381	18.672	-26.070
02:52:05.88	+00:17:05.7	1.4690	20.426	-24.390
02:53:33.54	+00:16:34.2	1.4530	20.479	-24.312

Table A.5: Table showing the position, redshift and magnitude of each quasar in the LQGs

RA	Dec	z	i	M_i
03:08:53.67	-00:18:01.9	1.4391	19.243	-25.503
03:09:16.05	+00:18:34.4	1.4324	20.339	-24.483
03:10:12.74	-00:11:49.5	1.4254	19.944	-24.792
03:10:13.60	-00:44:01.6	1.4111	19.940	-24.738
03:11:10.21	-00:10:15.0	1.4107	19.583	-25.119
03:12:06.49	+00:04:49.6	1.4097	19.591	-25.101
03:12:57.10	-00:19:27.8	1.4021	19.582	-25.104
03:13:07.92	-00:32:22.0	1.4104	19.072	-25.638
03:13:24.47	-01:11:33.6	1.4300	20.021	-24.711
03:13:25.57	-00:38:00.9	1.4303	18.817	-25.935
01:52:43.30	+01:12:18.7	1.4070	18.651	-25.941
01:53:13.28	+00:53:07.3	1.3988	19.561	-25.016
01:53:29.75	-00:22:14.3	1.3847	19.041	-25.532
01:53:51.64	+01:05:13.7	1.3896	19.876	-24.697
01:54:24.26	-00:25:53.2	1.4005	19.038	-25.560
01:54:56.10	+00:58:08.6	1.3784	19.569	-24.988
01:55:28.62	-00:38:56.7	1.3823	19.477	-25.084
01:56:05.95	+00:30:36.4	1.3882	20.417	-24.161
01:56:10.65	+01:11:59.5	1.3951	20.300	-24.282
01:56:14.76	-00:07:31.6	1.3821	19.289	-25.274
01:57:48.91	-00:20:04.5	1.3929	20.164	-24.402
01:14:11.77	+00:11:19.3	1.5287	18.211	-26.585
01:14:26.74	-00:14:51.2	1.5544	19.936	-24.899
01:14:57.36	+00:33:29.3	1.5424	20.170	-24.647
01:15:29.47	-00:57:23.7	1.5954	19.644	-25.277
01:15:40.05	-00:33:28.7	1.5930	17.930	-26.965
01:15:57.43	+00:07:25.9	1.5377	19.850	-24.967
01:16:22.74	-00:17:02.1	1.5677	19.679	-25.181
01:16:35.00	-00:50:26.0	1.5782	20.015	-24.875
01:16:37.95	+00:27:03.1	1.5249	20.222	-24.569
01:16:52.11	-00:06:15.2	1.5731	19.002	-25.866
01:17:12.38	-00:01:22.8	1.5326	20.148	-24.661
01:17:40.54	-00:02:50.4	1.5509	19.852	-24.992
01:18:58.27	-00:17:38.5	1.5421	20.485	-24.341
01:19:01.34	-00:07:07.8	1.5824	20.112	-24.775

TABLE A.6: Table showing the position, redshift and magnitude of each quasar in the LQGs

RA	Dec	z	i	M_i
01:30:37.53	-00:32:36.7	1.7433	19.899	-25.221
01:30:44.95	-00:47:49.7	1.7503	19.444	-25.663
01:31:35.93	-00:45:18.0	1.7250	19.931	-25.160
01:33:33.76	-00:55:11.1	1.7337	19.848	-25.261
01:33:35.75	-01:07:09.4	1.7934	20.358	-24.826
01:33:46.58	-00:47:29.5	1.7624	19.674	-25.466
01:34:07.28	-00:38:24.3	1.7778	20.264	-24.891
01:34:15.48	-00:55:41.0	1.7568	17.619	-27.512
00:51:14.50	+00:23:44.6	1.5655	20.319	-24.519
00:51:24.93	+00:30:33.1	1.6164	19.915	-24.996
00:51:42.21	+00:21:29.0	1.5511	19.948	-24.867
00:51:42.86	+00:57:50.9	1.5922	20.036	-24.853
00:52:06.98	+00:48:16.9	1.6003	20.094	-24.802
00:52:36.73	+00:32:34.2	1.5760	19.635	-25.223
00:53:05.28	+00:26:08.3	1.5417	20.309	-24.499
00:53:10.84	+00:30:25.6	1.5764	20.567	-24.293
00:53:19.94	+00:18:26.0	1.6067	19.832	-25.077
03:29:18.71	+00:36:44.6	1.7447	20.479	-24.903
03:30:04.34	+00:09:01.7	1.7968	19.257	-26.083
03:30:23.86	+00:36:41.4	1.7569	19.959	-25.365
03:30:36.46	+00:04:53.0	1.7954	19.635	-25.694
03:30:48.50	-00:28:19.6	1.7791	18.754	-26.548
03:31:14.69	+00:47:08.2	1.7718	20.077	-25.231
03:31:26.90	-00:00:09.9	1.7757	19.410	-25.877
03:31:31.18	-00:02:07.8	1.7714	19.489	-25.793
03:31:53.73	+00:20:26.6	1.7494	19.931	-25.321
01:04:58.02	+00:25:22.0	1.7563	19.933	-25.186
01:05:07.29	+00:24:40.5	1.7746	19.923	-25.217
01:07:05.96	+00:24:40.7	1.7663	19.725	-25.411
01:07:30.00	+00:03:56.8	1.7529	19.837	-25.28
01:08:10.52	+00:17:55.8	1.7876	20.132	-25.032
01:08:15.34	-00:18:02.8	1.7611	19.183	-25.957
01:09:15.79	-00:22:39.9	1.7672	19.698	-25.447
01:09:15.97	-00:32:04.6	1.7741	19.041	-26.124
01:09:47.74	-00:03:30.6	1.7510	19.447	-25.678
01:10:24.50	-00:15:43.8	1.7587	18.642	-26.489

Table A.7: Table showing the position, redshift and magnitude of each quasar in the LQGs

RA	Dec	z	i	M_i
00:30:56.58	+00:17:55.0	1.7495	19.743	-25.359
00:31:20.59	+00:00:42.2	1.7177	19.694	-25.363
00:31:27.25	-00:04:32.1	1.6909	19.371	-25.648
00:31:31.44	+00:34:20.2	1.7355	18.475	-26.608
00:31:49.99	-00:14:33.1	1.6770	19.978	-25.017
00:32:48.70	-00:23:58.3	1.6827	19.378	-25.63
00:33:03.93	+00:18:59.2	1.7387	20.076	-25.001
00:33:26.11	+00:07:41.6	1.7220	20.186	-24.869
00:33:38.32	-00:04:54.3	1.7435	19.877	-25.209
00:34:35.13	-00:09:47.8	1.6711	19.514	-25.47
00:35:00.61	-00:16:23.4	1.7204	19.916	-25.133
00:35:43.07	-00:10:43.2	1.7331	19.723	-25.347
03:30:06.75	+00:17:44.6	1.5156	20.718	-24.229
03:30:09.96	+00:08:35.6	1.5425	19.753	-25.228
03:30:16.60	+00:50:40.5	1.5223	20.560	-24.438
03:30:37.42	+00:35:53.9	1.5188	19.415	-25.555
03:30:40.02	+00:07:04.6	1.5098	18.499	-26.426
03:31:19.78	+01:12:56.5	1.5599	19.612	-25.443
03:31:24.59	-00:05:54.2	1.5096	18.696	-26.22
03:31:40.58	+00:20:06.4	1.5082	18.178	-26.731
03:31:59.28	+00:41:46.9	1.5581	20.541	-24.436
03:32:03.28	+00:34:24.0	1.5393	19.073	-25.876
03:32:17.08	+00:22:03.8	1.5313	19.242	-25.694
03:33:52.24	+00:33:58.3	1.5203	19.867	-25.079
03:19:08.22	+00:28:48.4	1.8182	19.590	-25.727
03:20:09.03	+00:34:04.2	1.8068	19.931	-25.413
03:20:15.79	+00:26:09.2	1.7605	19.799	-25.468
03:20:19.38	+00:36:02.6	1.7973	18.460	-26.88
03:20:22.76	+00:41:08.2	1.7868	17.849	-27.501
03:21:35.51	+00:34:56.9	1.8291	20.215	-25.168
03:22:00.45	+00:56:13.6	1.7537	19.713	-25.594
03:22:39.03	+00:49:45.6	1.7849	19.101	-26.234
03:23:08.71	+00:59:40.7	1.7371	19.580	-25.701
03:23:23.49	+00:30:14.9	1.8377	19.527	-25.858
03:23:44.58	+00:57:08.8	1.7697	19.412	-25.903
03:24:00.51	+00:49:24.8	1.7130	20.288	-24.94
03:24:39.63	+00:07:54.0	1.8306	20.167	-25.293

Table A.8: Table showing the position, redshift and magnitude of each quasar in the LQGs

RA	Dec	z	i	M_i
01:14:11.77	+00:11:19.3	1.5287	18.211	-26.585
01:14:26.74	-00:14:51.2	1.5544	19.936	-24.899
01:14:57.36	+00:33:29.3	1.5424	20.170	-24.647
01:15:17.79	+00:17:15.3	1.5846	19.886	-25.005
01:15:29.47	-00:57:23.7	1.5954	19.644	-25.277
01:15:40.05	-00:33:28.7	1.5930	17.930	-26.965
01:15:57.43	+00:07:25.9	1.5377	19.850	-24.967
01:16:22.74	-00:17:02.1	1.5677	19.679	-25.181
01:16:35.00	-00:50:26.0	1.5782	20.015	-24.875
01:16:37.95	+00:27:03.1	1.5249	20.222	-24.569
01:16:52.11	-00:06:15.2	1.5731	19.002	-25.866
01:17:12.38	-00:01:22.8	1.5326	20.148	-24.661
01:17:40.54	-00:02:50.4	1.5509	19.852	-24.992
01:18:58.27	-00:17:38.5	1.5421	20.485	-24.341
01:19:01.34	-00:07:07.8	1.5824	20.112	-24.775
02:15:10.26	-00:36:40.4	1.5363	20.1	-24.73
02:15:20.09	-00:02:09.0	1.6361	19.682	-25.288
02:16:10.30	-00:59:19.5	1.5239	19.438	-25.365
02:16:21.98	-01:08:18.5	1.5184	19.733	-25.059
02:16:30.25	-01:11:55.0	1.521	20.019	-24.775
02:16:49.25	-00:37:23.5	1.5421	18.621	-26.208
02:17:20.97	-00:13:23.8	1.6248	19.834	-25.109
02:17:34.63	-00:26:41.9	1.5567	18.155	-26.69
02:17:42.83	-01:14:14.7	1.5354	19.61	-25.206
02:18:14.08	+00:34:48.3	1.618	20.155	-24.802
02:18:25.32	+00:01:35.7	1.6169	20.424	-24.526
02:19:06.32	-00:12:24.7	1.5855	19.802	-25.096
02:19:46.51	-00:34:40.2	1.5678	19.564	-25.305
02:19:51.76	-00:21:08.2	1.6049	19.116	-25.808
02:20:48.33	-00:28:33.5	1.5447	20.01	-24.821
02:22:26.98	-00:07:38.1	1.5415	20.163	-24.67
02:22:28.46	-00:10:30.1	1.5397	19.773	-25.057
02:22:46.46	-00:48:36.1	1.5398	17.335	-27.493
02:23:04.23	+00:10:40.7	1.5509	19.266	-25.589
02:23:21.38	-00:07:33.8	1.5345	18.776	-26.054
02:24:00.23	-00:12:41.2	1.5697	20.039	-24.838
02:25:33.77	-00:14:13.5	1.5178	20.292	-24.499
02:25:36.28	-00:20:29.7	1.5378	20.046	-24.777

TABLE A.9: Table showing the position, redshift and magnitude of each quasar in the LQGs

RA	Dec	z	i	M_i
22:00:03.46	+00:53:32.3	1.54	20.097	-24.757
22:01:11.75	+00:34:26.7	1.5597	19.823	-25.077
22:01:18.07	-00:00:51.4	1.5626	20.249	-24.654
22:01:36.78	+00:36:46.0	1.5677	19.172	-25.733
22:01:52.38	-00:17:20.8	1.5809	20.533	-24.407
22:02:04.15	-00:20:43.6	1.5717	19.818	-25.11
22:03:24.15	-00:39:08.1	1.5708	19.32	-25.62
22:04:28.40	-00:43:29.3	1.5565	20.09	-24.861
22:06:32.56	-00:18:44.1	1.5496	18.813	-26.209
22:06:44.59	-00:38:53.2	1.5139	19.566	-25.389
22:08:01.01	-00:50:02.7	1.5495	20.049	-24.884
22:08:09.02	-00:40:23.4	1.5096	19.985	-24.88
22:08:54.39	-01:06:30.6	1.5298	19.80	-25.142
22:09:26.68	-00:39:03.2	1.5154	19.503	-25.398
22:09:47.95	-00:43:05.0	1.5097	20.247	-24.642
22:09:58.33	-00:57:29.8	1.5519	19.682	-25.301
23:45:21.15	+00:56:24.0	1.2722	19.834	-24.526
23:46:14.36	+00:58:14.9	1.2599	19.475	-24.867
23:46:58.53	+00:22:30.2	1.2533	19.229	-25.095
23:49:28.21	+00:04:10.3	1.2525	20.985	-23.344
23:49:29.48	-00:07:18.3	1.2590	20.229	-24.114
23:49:39.89	-00:13:15.3	1.2666	20.106	-24.254
23:49:49.61	+00:35:35.3	1.2437	17.934	-26.377
23:50:05.09	+01:15:00.2	1.2410	20.077	-24.21
23:52:17.25	+00:39:03.7	1.2433	17.687	-26.625
23:54:00.08	+00:57:40.8	1.2457	19.643	-24.682

Table A.10: Table showing the position, redshift and magnitude of each quasar in the LQGs

RA	Dec	z	i	M_i
22:08:29.61	-00:5024.7	0.7497	20.290	-22.903
22:11:42.93	-00:3846.0	0.7475	20.092	-23.083
22:11:46.16	-00:3513.5	0.7587	20.329	-22.892
22:13:02.57	+00:3015.9	0.7630	20.622	-22.545
22:13:41.48	-00:0645.5	0.7591	20.416	-22.798
22:16:20.26	-00:1632.3	0.7547	19.730	-23.482
22:17:07.16	-00:4721.9	0.7553	20.400	-22.837
22:17:15.18	+00:2615.0	0.7536	20.154	-22.997
20:48:13.65	-00:5701.8	0.6808	18.025	-24.92
20:48:57.53	-00:2538.4	0.6789	19.658	-23.283
20:52:11.05	-00:0557.3	0.6812	19.441	-23.601
20:52:12.82	+00:1137.4	0.6869	19.245	-23.796
20:53:43.56	+00:5344.3	0.6881	20.178	-22.808
20:54:33.03	+00:0602.0	0.6844	19.095	-23.89
20:55:21.73	+00:2423.2	0.6705	20.203	-22.715
20:55:46.82	+01:0434.4	0.6884	19.037	-23.966
20:56:23.36	+00:3544.0	0.6925	19.360	-23.637
23:22:54.33	-00:18:22.1	0.6233	19.429	-23.238
23:23:41.53	+00:27:24.0	0.6294	20.204	-22.487
23:24:38.51	-00:05:52.5	0.6114	19.701	-22.924
23:25:29.43	-00:47:35.0	0.6294	19.825	-22.867
23:26:52.96	-00:30:12.6	0.6059	19.513	-23.081
23:28:03.53	-00:16:56.3	0.6342	19.650	-23.054
23:29:02.89	-00:27:16.9	0.6191	19.770	-22.875
23:31:29.83	-00:49:33.3	0.6149	18.600	-24.017
23:31:33.07	-00:56:09.1	0.6382	19.214	-23.501
23:32:58.90	-01:05:56.6	0.6035	19.997	-22.577
23:37:05.35	+00:50:02.8	0.7091	19.309	-23.661
23:37:06.36	+00:21:32.3	0.7130	19.744	-23.238
23:37:13.66	+00:56:10.8	0.7081	18.735	-24.236
23:39:52.77	-00:08:40.0	0.7118	19.818	-23.154
23:39:55.84	+01:02:58.5	0.7200	20.065	-22.925
23:40:09.91	+00:56:19.9	0.7158	18.762	-24.216
23:40:57.01	-01:12:46.1	0.7150	19.792	-23.185
23:41:45.81	-00:39:34.6	0.7201	19.662	-23.328
23:42:05.74	-00:36:33.6	0.7214	19.940	-23.057
23:45:02.73	-00:11:26.5	0.7275	19.822	-23.213

Table A.11: Table showing the position, redshift and magnitude of each quasar in the LQGs

Appendix B

Tables of Results of the full list of Mg II Absorbers found

Ra(J2000)	Dec(J2000)	zqso	zabs	nabs
343.03	0.98	1.71	0.80	1
343.39	-1.12	1.00	0.75	1
343.44	-0.80	2.14	1.93	1
343.57	-0.53	1.06	0.64	1
343.61	-1.22	2.35	1.06	1
343.62	0.02	1.63	1.11	1
343.63	-0.39	1.94	0.80	1
343.93	-1.12	1.55	1.17	1
343.96	-0.15	2.01	1.38	1
344.04	1.10	2.27	1.95	1
344.08	-0.76	1.73	1.13	1
344.19	-0.84	0.52	0.38	1
344.28	-0.43	1.99	1.26	2

TABLE B.1: Table showing the position, redshift of the quasar, redshift of the absorbers and and the number of absorbers associated with the quasar.

Ra(J2000)	Dec(J2000)	zqso	zabs	nabs
344.39	-1.16	1.77	1.54	2
344.39	-1.16	1.77	1.00	2
344.45	0.02	1.71	1.24	2
344.45	0.02	1.71	1.55	2
344.47	0.38	3.29	1.50	2
344.47	0.38	3.29	1.48	2
344.57	-0.56	2.43	1.27	1
344.58	-0.06	2.37	1.40	1
344.62	0.39	3.13	1.65	1
344.76	0.54	1.46	1.37	1
345.05	1.12	1.79	0.82	1
345.14	-0.82	2.21	1.44	1
345.14	1.25	1.88	1.66	1
345.24	-0.86	3.17	1.43	1
345.27	-0.40	1.88	0.64	1
345.28	-0.39	1.79	1.20	2
345.28	-0.39	1.79	0.61	2
345.33	1.01	2.07	1.54	1
345.34	-0.73	1.97	1.05	2
345.38	-0.12	2.10	1.92	2
345.38	-0.12	2.10	1.84	2
345.51	0.25	1.67	0.94	1
345.53	0.56	1.07	0.44	1
345.55	1.01	2.01	0.88	2
345.55	1.01	2.01	1.29	2
345.61	-0.45	1.37	1.07	1
345.85	0.69	1.80	1.32	1
346.00	-0.68	1.07	0.65	1
346.01	0.03	1.59	1.23	2
346.01	0.03	1.59	0.85	2

Table B.2: Table showing the position, redshift of the quasar, redshift of the absorbers and and the number of absorbers associated with the quasar.

Ra(J2000)	De(J2000)	zqso	zabs	nabs
353.06	-0.91	1.83	1.38	2
353.12	0.01	1.60	0.62	2
353.12	0.01	1.60	0.83	2
353.46	-0.57	2.00	1.38	2
353.46	-0.57	2.00	1.87	1
353.61	1.27	2.96	2.24	1
353.67	0.87	1.04	0.47	2
354.00	-0.93	1.30	0.48	2
354.00	-0.93	1.30	0.41	1
354.01	0.39	2.15	1.14	2
354.05	-1.23	1.51	1.10	2
354.05	-1.23	1.51	0.81	1
354.07	-1.10	1.87	1.51	1
354.08	-0.30	2.14	1.81	1
354.11	-0.13	0.74	0.41	2
354.15	-1.13	1.30	0.80	1
354.24	1.09	1.09	0.79	1
354.24	0.35	1.93	1.55	1
354.25	0.92	2.11	1.04	1
354.32	-0.35	2.18	1.87	1
354.47	-0.11	1.78	1.47	1
354.58	-0.94	0.89	0.48	2
354.66	-0.59	2.67	1.85	2
354.66	-0.59	2.67	1.30	3
354.67	0.39	1.47	0.47	3
354.67	0.39	1.47	0.43	3
354.67	0.39	1.47	1.42	2
354.79	0.64	1.25	0.78	2
354.79	0.64	1.25	1.13	1
354.82	-0.50	1.34	0.97	1
354.88	0.50	3.05	2.05	1
354.97	0.49	1.57	1.32	1
355.01	-0.88	2.26	2.02	1

Table B.3: Table showing the position, redshift of the quasar, redshift of the absorbers and and the number of absorbers associated with the quasar.

Ra(J2000)	Dec(J2000)	zqso	zabs	nabs
37.94	0.46	1.49	0.52	1
37.96	1.27	1.95	1.42	2
37.96	1.27	1.95	1.60	2
38.02	0.55	0.92	0.78	1
38.02	1.11	1.26	0.48	3
38.02	1.11	1.26	0.85	3
38.04	-0.13	1.36	0.56	3
38.04	-0.13	1.36	0.98	3
38.07	0.37	1.75	1.31	2
38.07	0.37	1.75	1.01	2
38.08	0.35	2.04	1.31	2
38.08	0.35	2.04	2.00	2
38.11	-0.20	1.73	0.69	1
38.14	0.14	2.66	1.69	1
38.22	-0.78	1.81	0.99	1
38.26	-1.25	2.50	2.10	2
38.26	-1.25	2.50	1.00	2
38.36	0.49	2.01	0.71	2
38.36	0.49	2.01	1.05	2
38.39	1.06	2.06	1.78	3
38.39	1.06	2.06	0.92	3
38.39	1.06	2.06	0.83	3
38.50	0.83	2.53	1.97	1
38.84	0.09	1.38	0.56	1
39.02	-0.51	1.40	0.82	2
39.02	-0.51	1.40	1.36	2
39.03	0.93	0.96	0.82	1
39.93	0.11	3.62	1.59	1

TABLE B.4: Table showing the position, redshift of the quasar, redshift of the absorbers and and the number of absorbers associated with the quasar.

Ra(J2000)	Dec(J2000)	zqso	zabs	nabs
40.03	-0.34	1.70	1.51	1
40.04	-0.58	1.51	1.18	1
40.04	-1.11	1.82	1.51	2
40.04	-1.11	1.82	1.53	2
40.16	0.42	1.72	0.57	1
40.40	-0.15	0.82	0.43	1
40.43	0.98	1.89	1.51	1
40.49	0.12	1.56	0.98	1
40.54	1.23	1.65	1.57	1
40.63	-0.01	2.49	1.56	1
40.75	-0.18	2.00	1.33	1
40.77	0.00	2.00	1.05	1
40.78	-0.43	1.28	0.78	2
40.78	-0.43	1.28	0.58	2
40.91	0.74	2.42	1.36	1
40.92	-0.30	1.43	0.60	1
40.99	-1.23	0.90	0.81	1

Table B.5: Table showing the position, redshift of the quasar, redshift of the absorbers and and the number of absorbers associated with the quasar.

Ra(J2000)	Dec(J2000)	zqso	zabs	nabs
41.01	1.22	1.57	1.30	1
41.09	-1.21	1.65	0.50	1
41.11	-0.51	2.08	0.87	1
41.21	-0.83	2.42	1.36	1
41.32	1.24	1.44	1.06	1
41.37	-1.10	1.69	1.41	1
41.39	1.14	1.52	1.11	1
41.46	-0.01	1.29	0.83	1
41.48	-0.12	1.65	1.31	1
41.49	-0.14	2.20	1.61	2
41.49	-0.14	2.20	1.54	2
41.52	-0.54	1.60	0.85	1
41.53	-0.93	1.43	0.83	1
41.55	-0.53	1.74	0.84	1
41.55	0.40	1.58	0.93	2
41.55	0.40	1.58	0.82	2
41.56	0.91	3.02	1.37	2
41.56	0.91	3.02	1.44	2
41.62	-0.75	2.11	1.24	1
41.64	-0.54	2.15	2.11	2
41.64	-0.54	2.15	1.94	2
41.66	-0.68	0.86	0.70	1
41.71	-0.75	2.19	1.24	3
41.71	-0.75	2.19	1.34	3
41.71	-0.75	2.19	1.71	3
41.77	0.31	0.65	0.58	1
41.80	0.86	1.60	1.38	2
41.80	0.86	1.60	1.07	2
41.91	-0.08	1.85	1.23	1
41.96	-1.14	1.60	0.97	1
41.98	-0.27	2.13	1.65	1
42.07	0.49	1.03	0.81	1
42.09	0.17	1.64	0.59	1
42.13	0.83	1.60	0.91	1
42.14	-0.77	1.83	1.36	2
42.14	-0.77	1.83	1.18	2

TABLE B.6: Table showing the position, redshift of the quasar, redshift of the absorbers and and the number of absorbers associated with the quasar.

Bibliography

Adami, C., Mazure, A., 1999, A&AS, 134, 393

Antonucci, R., 1993, ARAA, 31,473

Bardeen, J.M., Bond, J.R., Kaiser, N.,Szalay, A.S., 1986, AJ, 304, 15

Barrow, J.D., Bhavsar, S.P., Sonoda, D.H., 1985, MNRAS, 216, 17

Bhavsar, S.P., Splinter, R.J., 1996, MNRAS, 282, 1461

Bond, J.R., Cole. S., Efstathiou. G., Kaiser. N., 1991, ApJ, 379, 440

Caccianiga, A., Severgnini, P., Braito, V., Della Ceca, R., Maccacaro, t., et al., 2004, A&A, 416, 901

Clowes, R.G.,Campusano, L.E., 1991,MNRAS, 249, 218

Clowes, R.G.,Campusano, L.E., 1994, MNRAS, 266, 317

Clowes, R.G., Campusano, L.E., Sochting, I.K., Graham, M.J., 2012, MNRAS, 419, 556

Clowes, R.G., Harris, K.A., Raghunathan, S., Campusano, L.E., Sochting, I.K., Graham, M.J., 2013, MNRAS, 429, 2910

Coil, A.L., et al., 2009, ApJ, 701, 1484

Coil, A.L., Hennawi, J.F., Newman, J.A., Cooper, M.C., Davis, M., 2007, ApJ, 654, 115

Coles, P., Lucchin, F., 1995, coec, book, Cosmology, The origin and evolution of cosmic structure

Crampton, D.,Cowley, A.P.,Hartwick, F.D.A., 1989,, 345, 59

Croom, S.M.,Smith, R.J.,Boyle, B.J.,Shanks, T.,Miller, L.,Outram, P.J.,Loaring, N.S., 2002, MNRAS, 335, 459

Croom, S.M.,Smith, R.J.,Boyle, B.J.,Shanks, T.,Miller, L.,Outram, P.J.,Loaring, N.S., 2004, MNRAS, 349, 1397

Croton, D.J., et al. 2006,MNRAS, 367, 864

De Lucia, G., Springel, V., White, S.D.M., Croton, D., Kauffmann, G., 2006, ApJS, 162, 428

Doroshkevich, A.G., Muller, V., Retzlaff, J., Turchaninov, V., 1999, MNRAS, 306, 575

Efstathiou, G., Bridle, S.L., Lasenby, A.N., Hobson, M.P., Ellis, R.S., 1999, MNRAS, 303, 47 Einasto, M.,2008, ApJ, 685, 83

Fan, X., et al., 2001, AJ, 121, 54

Ferrarese, L., Ford, H., 2005, SSRv, 116, 523

Ferrarese, L., Merritt, D., 2000, Apj, 539, 9

Fiore, F., Brusa, M., Cocchia, F., Baldi, A., et al., 2003, A&A, 209, 79

Fosalba, P., Gaztanaga, E., Castander, F.J., Manera, M., 2008, MNRAS, 391, 435

Fukugita, M., Ichikawa, T., Gunn, J.E., Doi, M., Shimasaku, K., Schneider, D.P., 1996, AJ, 111, 1784

Gebhardt, K., et al., 2000, ApJ, 539, 13

Georgakakis, A., Nandra, K., Laird, E. S., et al. 2006, MNRAS, 371, 221

Graham, M.J., Clowes, R.G.,Campusano,L.E., 1995, MNRAS, 275, 790

Gunn, J.E., et al., 1998, AJ, 116, 304 Hewett,P.C., Foltz, C.B., Chaffee, F.H., 1995, AJ, 109, 1498

Hewett, P.C., Wild, V., 2010, MNRAS, 405, 2302

Hopkins. P.F., Hernquist, L., Cox, T.J., Di Matteo, T., Robertson, B., & Springel, V. 2006., ApJS, 163, 1

Hopkins, P.F, Herquist, L., Cox, T.J., Robertson, B., Di Matteo, T., Springel, V., Martini, P., Somerville, R., Li, Y., 2005, AAS, 20711604

Hopkins, P.F., Hernquist, L., Cox, T.J., Keres, D., 2008, ApJS, 175, 356

Kauffmann, G., Haehnelt, M., 1999, AAS, 195

Kauffmann, G., Haehnelt, M., 2000, MNRAS, 311, 576

Kauffmann, G., Haehnelt, M.G.,2002, MNRAS, 332, 529

Krzewina, L.G., Saslaw, W.C., MNRAS, 1996, 278, 869

Kromberg, B.V., Kravtsov, A.V., Lukash, V.N., 1996, MNRAS, 282, 713

Kruskal, J.B., 1956, Proc, Am, Math, Soc, 7,48

Kromberg. B.V., Kravtsov. A.V., Lukash. V.N., 1996, MNRAS, 282, 713

Lacey. C., Cole, S., 1993, MNRAS, 262, 627-649

Lemon, G., & Virgo Consortium., 2006, preprint(astro-ph/0608019

Lidz, A., Hopkins, P.F., Cox. T.J., Hernquist, L., Robertson. B., 2006, ApJ, 641, 41

Mandelbaum, R., McDonald, P., Seliak. U., Cen, R.,2003, MNRAS, 344, 776

Martinez-Sansigre, A., Rawlings, S., Lacy, M., Fadda, D., Marleau, F., et al., 2005, Nature, 436, 7051, 666

Mshar, A.C., Charlton, J.C., Lynch, R.S., Churchill, C., Kim, T.S., 2007, ApJ, 669, 135

Nadathur, S., 2013, MNRAS, 434, 398

Peacock, J.A., Cosmological Physics, (Cambridge University Press, Cambridge, U.K.;New York, U.S.A., 1999)

Peebles, P.J.E., Principles of Physical Cosmology (Princeton University Press, Princeton, U.S.A., 1993)

Percival, W.J., Sutherland, W., Peacock, J.A., et al., 2002, MNRAS, 337, 1068-1080

Planck Collaboration XXIII., 2013, A&A, 571, A23

Pilipenko, S.V., 2007, ARep, 51, 820

Press, W., & Schechter, P., 1974, ApJ, 187, 425

Prim, R.C., 1957, Bell Sys, Tech, J., 36, 1389

Richards, G.T., et al., 2006, ApJS, 166, 470

Richards, G., Vanden Berk, D., Reichard, T., et al., 2002, AJ, 124, 1

Richstone, D., et al., 1998, Natur, 395A, 14

Schawinski, K., Dowlin, N., Thoma,s D., Urry, C. M., Edmondson, E., 2010, ApJ, 714, L108

Sheth, R.K., Van de Weygaert. R., 2004, MNRAS, 350, 517

Shen, S., White, S.D.M., Mo, H.J., Voges, W., Kauffmann, G., Tremonti., C., Scott, F.A, 2006, MNRAS, 369, 1639

Shen, S., Kauffmann, G., Von der Linden, A., White, S.D.M., Best, P.N., 2008, MNRAS, 389, 1074

Shimasaku, K., Hayashino, T., Matsuda, Y., Ouchi, M., Ohta, K., Okamura, S., Tamura, H., Yamada, T., Yamauchi., 2004, ApJ, 605, L93

Steidel, C.C., Sargent, W.L., 1992, ApJS, 80, 108

Spergel, D.N., et al., 2003, ApJS, 148, 175

Sunyaev, R.A., and Zel'dovich, Ya. B.,1970, Comm. Astrophys. Space Phys. 4, 173

Sunyaev, R.A., and Zel'dovich, Ya. B., 1972

Spinger, V., 2005, MNRAS, 364, 1105

Taylor, K., Cannon, R., Watson, D., Frederick, G., 1997, SPIE, 2871, 145

Tasse, C., Cohen, A.S., Rottgering, H.J.A., Kassim, N.E., Perley, R., et al., 2006, A&A, 456, 791

Tegmark, M., et al., 2004, ApJ, 606, 702

Teyssier, R., Pires, S., Prunet, S., Aubert, D., Pichon, C., Amara, A., et al., 2009, A&A, 497, 335

Thacker, R.J., Scannapieco, E., Couchman, H.P., Richardson, M., 2009, ApJ, 693, 552

Voit, M.G., 2005, RvMP, 77, 207

Wang, J. X., Zheng, Z. Y., Malhotra, S., et al. 2007, ApJ, 669, 765

Webster, A.S.,1982, MNRAS, 199, 683

Williger, G.M., Campusano,L.E., Clowes, R.G. Graham, M.J., 2002, ApJ, 578, 708

Wray, J.J., Bahcall, N.A., Bode, P., Boettiger, C., Hopkins, P.F., 2006, ApJ, 652, 907

Zhu, G., Menard, B., 2013, ApJ, 770, 130